genes

MDPI

Article

Single-Cell RNA-Seq Analysis Reveals Lung Epithelial Cell Type-Specific Responses to HDM and Regulation by Tet1

Tao Zhu [1,†], Anthony P. Brown [1,†], Lucy P. Cai [1], Gerald Quon [2] and Hong Ji [1,3,*]

[1] California National Primate Research Center, University of California, Davis, CA 95616, USA; taozhu@ucdavis.edu (T.Z.); apbrown@ucdavis.edu (A.P.B.); lpcai@ucdavis.edu (L.P.C.)
[2] Department of Molecular and Cellular Biology, Genome Center, University of California, Davis, CA 95616, USA; gquon@ucdavis.edu
[3] Department of Anatomy, Physiology and Cell biology, School of Veterinary Medicine, University of California, Davis, CA 95616, USA
* Correspondence: hgji@ucdavis.edu; Tel.: +1-530-754-0679
† These authors contributed equally to this work.

Abstract: Tet1 protects against house dust mite (HDM)-induced lung inflammation in mice and alters the lung methylome and transcriptome. In order to explore the role of Tet1 in individual lung epithelial cell types in HDM-induced inflammation, we established a model of HDM-induced lung inflammation in Tet1 knockout and littermate wild-type mice, then studied EpCAM$^+$ lung epithelial cells using single-cell RNA-seq analysis. We identified eight EpCAM$^+$ lung epithelial cell types, among which AT2 cells were the most abundant. HDM challenge altered the relative abundance of epithelial cell types and resulted in cell type-specific transcriptomic changes. Bulk and cell type-specific analysis also showed that loss of Tet1 led to the altered expression of genes linked to augmented HDM-induced lung inflammation, including alarms, detoxification enzymes, oxidative stress response genes, and tissue repair genes. The transcriptomic regulation was accompanied by alterations in TF activities. Trajectory analysis supports that HDM may enhance the differentiation of AP and BAS cells into AT2 cells, independent of Tet1. Collectively, our data showed that lung epithelial cells had common and unique transcriptomic signatures of allergic lung inflammation. Tet1 deletion altered transcriptomic networks in various lung epithelial cells, which may promote allergen-induced lung inflammation.

Keywords: allergic lung inflammation; Tet1; single-cell RNA-seq; alveolar type 2 (AT2) cells; ciliated cells

check for updates

Citation: Zhu, T.; Brown, A.P.; Cai, L.P.; Quon, G.; Ji, H. Single-Cell RNA-Seq Analysis Reveals Lung Epithelial Cell Type-Specific Responses to HDM and Regulation by Tet1. *Genes* **2022**, *13*, 880. https://doi.org/10.3390/genes13050880

Academic Editors: Asunción García-Sánchez and Catalina Sanz

Received: 4 April 2022
Accepted: 11 May 2022
Published: 14 May 2022

Publisher's Note: MDPI stays neutral with regard to jurisdictional claims in published maps and institutional affiliations.

Copyright: © 2022 by the authors. Licensee MDPI, Basel, Switzerland. This article is an open access article distributed under the terms and conditions of the Creative Commons Attribution (CC BY) license (https://creativecommons.org/licenses/by/4.0/).

1. Introduction

Asthma is one of the most common pulmonary disorders with high heterogeneity [1]. Previous studies have noted transcriptomic differences in both asthmatic patients and animals with allergic lung inflammation [2–4]. Recent studies, including ours [2,5–7], have linked DNA methylation-associated transcriptomic changes to the pathogenesis and progression of asthma. Other studies have linked enzymes involved in DNA methylation maintenance to asthma pathogenesis [8]. Our studies in pediatric nasal epithelial samples and bronchial epithelial cells (HBECs) [9–11] suggest that Tet1 (Tet Methylcytosine Dioxygenase 1) may regulate childhood asthma and responses to environmental exposures. Tet1 is a ten-eleven translocation methylcytosine dioxygenase. These demethylases catalyze the hydroxylation of DNA methylcytosine (5mC) into 5-hydroxymethylcytosine (5hmC), 5-formylcytosine (5fC), and 5-carboxycytosine (5caC), interact with histone modifiers and transcription factors, and contribute to many biological processes and responses to environmental exposures (reviewed in [12]). In a follow-up study using genetic knockout mice [9], we found that Tet1 plays a protective role in allergic lung inflammation. Tet1 knockout mice exhibited significantly increased IL13 and IL33 (mRNA and protein levels) in the

lungs. Concurrent with increased lung inflammation following house dust mite (HDM) challenges, Tet1 knockout mice showed a dysregulated expression of genes in several signaling pathways, including NRF2-mediated oxidative stress response, aryl hydrocarbon receptor (AhR) signaling, and interferon (IFN) signaling. These genes were also regulated by Tet1 in HBECs [9].

Given the use of RNA from total mouse lung tissues in these previous studies, critical questions remained regarding the cellular origin(s) of inflammatory mediators and molecules (e.g., IL33) following allergen challenges, and the role that Tet1 plays in regulating these mediators/molecules in individual cell types in vivo. In this study, our primary goal was to identify epithelial cell types that were influenced by HDM treatment and Tet1 knockout in vivo using single-cell RNA-seq analysis. We hypothesized that Tet1 regulates genes in proinflammatory and oxidative stress response pathways in specific lung epithelial cells, and that the loss of Tet1 has similar effects on these pathways compared to HDM treatment. The transcriptomic effects of Tet1 loss and HDM challenges were compared in all EpCAM$^+$ cells together and in each cell type, and the effects of Tet1 loss in the presence of HDM was also evaluated. We observed similar effects of Tet1 deficiency and HDM on the transcription of alarmins and detoxification enzymes, as well as of the down-regulation of oxidative stress pathways and the upregulation of markers of epithelial injury following Tet1 knockout in the presence of HDM. These data suggest possible pathways through which Tet1 protects against HDM-induced lung inflammation.

2. Methods

2.1. Establishment of HDM-Induced Airway Inflammation Mouse Model and Isolation of EpCAM$^+$ CD31$^-$ CD45$^-$ (EpCAM$^+$) Lung Epithelial Cells

HDM-induced allergic inflammation was established in both Tet1$^{-/-}$ mice (knockout/KO mice) and their littermate Tet1$^{+/+}$ mice (wild-type/WT mice), as described in a previous study [9] (details in Supplementary Materials and Figure S1A). All animal procedures were approved by the Institutional Animal Care and Use Committee at the University of California, Davis. The mice were divided into 4 groups, WT-Saline, WT-HDM, KO-Saline, and KO-HDM, with 2 mice in each. Airway inflammation was assessed by histology. Lobes, about 5 mm large, were sectioned in half and collected from each animal. Lobes from animals of the same group were pooled. Tissues were minced in a collagenase (480 U/mL)–dispase (5 U/mL)–DNase (80 U/mL) digestion solution in DPBS with Ca^+ and Mg^{2+} and razor blades. The finely minced tissues were incubated in 6mL of digestion solution at 37 °C for 40 min, with gentle inversion for 30 s at 5 min intervals. After incubation, samples were washed with a DPBS/1% BSA wash buffer and passed through a 70 µm filter strainer. After spinning down cells and removing the supernatant, cells were treated with AKC lysis buffer to remove red blood cells, and washed once more to remove dead cells and excess RNA in the buffer. CD45$^+$ cells (immune cells) and CD31$^+$ (endothelial cells) were then depleted using mouse CD45 and CD31 MicroBeads (Miltenyi Biotec), and the remaining cells were counted and incubated with anti-CD326-APC (eBioscience), anti-CD31-PE-cy7 (eBioscience), and anti-CD45-PE (Biolegend). CD326$^+$ CD31$^-$ CD45$^-$ cells were collected on a MoFlo sorter (Beckman Coulter/MoFlo XDP) with >99% purity at the Research Flow Cytometry Core at Cincinnati Children's Hospital Medical Center (Figure S1B).

2.2. Single-Cell Library Preparation and Sequencing

For 10X Genomics single-cell RNA sequencing, cells were brought to a concentration of about 1000 cells/µL using the resuspension buffer. A total of 8000 cells were targeted for cDNA preparation and put through the 10X Genomics Chromium Next GEM Single Cell 3′ v3.1 (Pleasanton, CA, USA) pipeline for library preparation. After cDNA preparation and GEM generation and clean-up, cDNA was quality checked and quantified on an Agilent Bioanalyzer DNA High-Sensitivity chip at a 1:10 dilution. Successful traces showed a fragment size range of approximately 1000–2000 bp. A total of 12 indexing cycles for the library were used. The quality of the indexed libraries was checked on an Agilent

Bioanalyzer DNA High-Sensitivity chip at a 1:10 dilution. Successful libraries had fragment size distributions with peaks around 400bp. Libraries were sequenced using 4 Illumina Hiseq lanes (Paired-end 75 bp).

2.3. Single-Cell RNA-Sequencing Data Analysis

We used Cell Ranger v3.1.0 [13] for initial processing of the scRNA-seq data. Specifically, we used Cell Ranger for sample demultiplexing, barcode processing, read alignment to the reference genome, data aggregation, and generating expression matrices. We then imported the data into Seurat v3.1.4 [14] for downstream processing. Cells that had fewer than 700 genes expressed, greater than 10% of reads mapping to the mitochondria, fewer than 20,000 unique molecular identifiers, or that expressed Pecam1 (CD31, an endothelial marker [15]) were filtered out. We also used cell cycle markers to identify which part of the cell cycle each cell was in during sampling [16], and subsequently regressed out this variable and the percentage of mitochondrial reads in each cell while normalizing and scaling the data with Seurat. In order to cluster all cell types accurately without biases from the HDM treatment, we used scAlign [17], a program that uses an unsupervised deep learning algorithm to correct for treatment effects that can affect cell clustering. First, the data were separated into two separate files based on treatment, and 3000 variable features were identified in each file separately. Variable features that overlapped were used for downstream clustering. We then performed single-cell alignment by performing a bidirectional mapping between cells with different treatments, creating a low-dimensional alignment space where cells were grouped together by type rather than by treatment [17]. Our best results (i.e., greatest separation of clusters by type rather than by treatment) were achieved by using the first 50 principal component scores, rather than individual gene-level data, as model inputs. The output from the scAlign model was subsequently used as the input for a uniform manifold approximation and projection (UMAP) in Seurat [14] to visualize the cell clusters.

We used the FindClusters function from Seurat to cluster the cells, using a wide range of resolutions, from 0.01 to 2, to identify the best resolution for our dataset. FindClusters is a shared nearest-neighbor modularity optimization-based clustering algorithm. Our eventual selection was a resolution of 1, yielding 11 initial cell clusters. We then used markers from the single-cell mouse cell atlas [18] and another study on lung epithelial cells [19] to identify cell clusters. For each cluster, we plotted the gene expression levels of the markers from each epithelial cell type in our references, and identified which cell type was represented by each cluster. We merged some of the original 11 clusters identified by Seurat [14] that expressed similar markers, only merging sister nodes in the cell cluster tree generated by BuildClusterTree from Seurat. After merging similar clusters, we had a total of nine different labeled cell clusters in our dataset. We then used Seurat to calculate cluster means and perform differential expression analyses via the Wilcoxon rank sum test. For each individual cell type, as well as for all cells combined, we performed five differential expression comparisons: (1) WT-HDM vs. WT-Saline (WT-Sal), (2) KO-Saline (KO-Sal) vs. WT-Sal, (3) KO-HDM vs. KO-Sal, (4) KO-HDM vs. WT-HDM, and (5) KO-HDM vs. WT-Sal. Differentially expressed genes (DEGs) had a false discovery rate (FDR) of 0.05 or less, and a fold change of at least 1.2. DEGs also had to be expressed in at least ten percent of one of the comparison groups to qualify as differentially expressed. Pathway enrichment analyses for DEGs from each comparison were performed using IPA (QIAGEN Inc. Germantown, MD, USA, https://digitalinsights.qiagen.com/products-overview/discovery-insights-portfolio/analysis-and-visualization/qiagen-ipa/) (accessed between 1 March 2021 and 1 April 2022).

2.4. Transcription Factor Activity Analysis

We used DoRothEA [20–22] to assess the relative transcription factor (TF) activity levels in different cell types and/or treatments. DoRothEA computes activity levels for transcription factors using the expression levels of targets of each TF, instead of the ex-

pression level of the TF itself. For our analysis, we chose to include only highly confident interactions between TFs and target genes (confidence levels "A", "B", or "C"). We used VIPER for statistical analysis of the TF activity levels, as VIPER considers the mode of each TF–target interaction and has been shown to be appropriate for single-cell analysis [22,23]. We compared the TF activity between cell types and plotted the top 50 by activity level variance. We also compared the TF activity within cell types by sample type in AT2 and ciliated cells, and plotted the top 25.

2.5. Single-Cell Trajectory Analysis

In order to assess the differentiation of AP and BAS cells to AT2 cells, we performed single-cell trajectory analysis using Monocle [24]. First, the dataset was divided to include only AP, BAS, and AT2 cells using Seurat [14]. Next, cells were ordered based on the progress they had made through the differentiation process via reversed graph embedding using Monocle; then, dimensionality reduction was performed using the "DDRTree" reduction method, and cell trajectories were visualized. We also performed trajectory analyses on different subsets of AP, BAS, and AT2 cells to better understand how HDM treatment and Tet1 deletion impacted the differentiation of AP and BAS cells into AT2 cells. We performed cell trajectory analyses on (1) all AP, BAS, and AT2 cells; (2) only wild-type AP, BAS, and AT2 cells; (3) only AP, BAS, and AT2 cells that had Tet1 knocked out; (4) only saline-treated AP, BAS, and AT2 cells; (5) only HDM-treated AP, BAS, and AT2 cells. For each of these comparisons, we also performed branched expression analysis modeling within Monocle to identify genes that were differentially expressed along the trajectory at branch points that roughly separated AP, BAS, and AT2 cells. However, this was not possible in the saline-cell-only group, as there were no branch points that clearly separated these different groups of cells. We then used Monocle to make heatmaps, to visualize the expression patterns of genes that showed a significant change in expression along these trajectories ($q < 1 \times 10^{-4}$).

3. Results

3.1. Single-Cell Analysis Identified Nine Cell Types in the EpCAM$^+$ CD45$^-$ CD31$^-$ Cells from Mouse Lungs

To identify cell types that are important in responses to HDM challenges and that are subject to Tet1 regulation, we isolated EpCAM$^+$ CD45$^-$ CD31$^-$ (referred to as EpCAM$^+$) lung epithelial cells from animals in an established HDM-induced allergic airway inflammation model [9] and characterized them using single-cell RNA-seq (overall study design in Figure 1A, treatment protocol and isolation strategy in Figure S1A,B). To demonstrate the successful establishment of allergen-induced lung inflammation, pathological alterations were observed. Consistent with previous observations [9], airway inflammatory cell infiltration, goblet cell proliferation, smooth muscle hypertrophy, and airway basement membrane thickening were observed in HDM-challenged WT (WT-HDM) mice included in the single-cell analysis (Figure S1C,D). Slightly more inflammatory cell infiltration, goblet cell proliferation, and airway mucus secretion were observed in HDM-challenged KO mice (KO-HDM) that were included in this scRNA-seq analysis. No pathological changes were observed in saline-treated mice.

Among the 25,437 cells that passed our quality filters, we identified 9 cell types (Figure 1B,C) based on established marker expression (Figure 1D, Table S1). As expected, most of the cell types expressed the respiratory epithelial cell markers *Epcam* and *Scgb1a1* (Figure S2). Interestingly, Tet1 was found to be mostly expressed in AT2 cells, alveolar progenitor cells, bronchial stem cells, ciliated cells, and club cells. In order of abundance, we identified AT2, alveolar progenitor (AP), broncho alveolar stem (BAS), ciliated, stromal, club, goblet, neuroendocrine, and AT1 cells (Figure 2 and Table S2). On average, we observed a 24.9% increase in AP cells and an 11.1% increase in BAS cells following HDM challenges, while there was a 29.2% and 3.1% decrease in AT2 and ciliated cells, respectively, following HDM challenges (Figure 2 and Table S2). There was also a small increase in the

percentage of goblet cells following HDM challenges, consistent with goblet cell metaplasia in histological studies (Figure S1C,D). Although we expected cell loss during single-cell preparation, especially for fragile AT1 cells, these results suggest dynamic changes in lung epithelial cell proportions in HDM-induced lung inflammation. Additionally, since stromal cells are not epithelial cells, we will not discuss DEGs in stromal cells further.

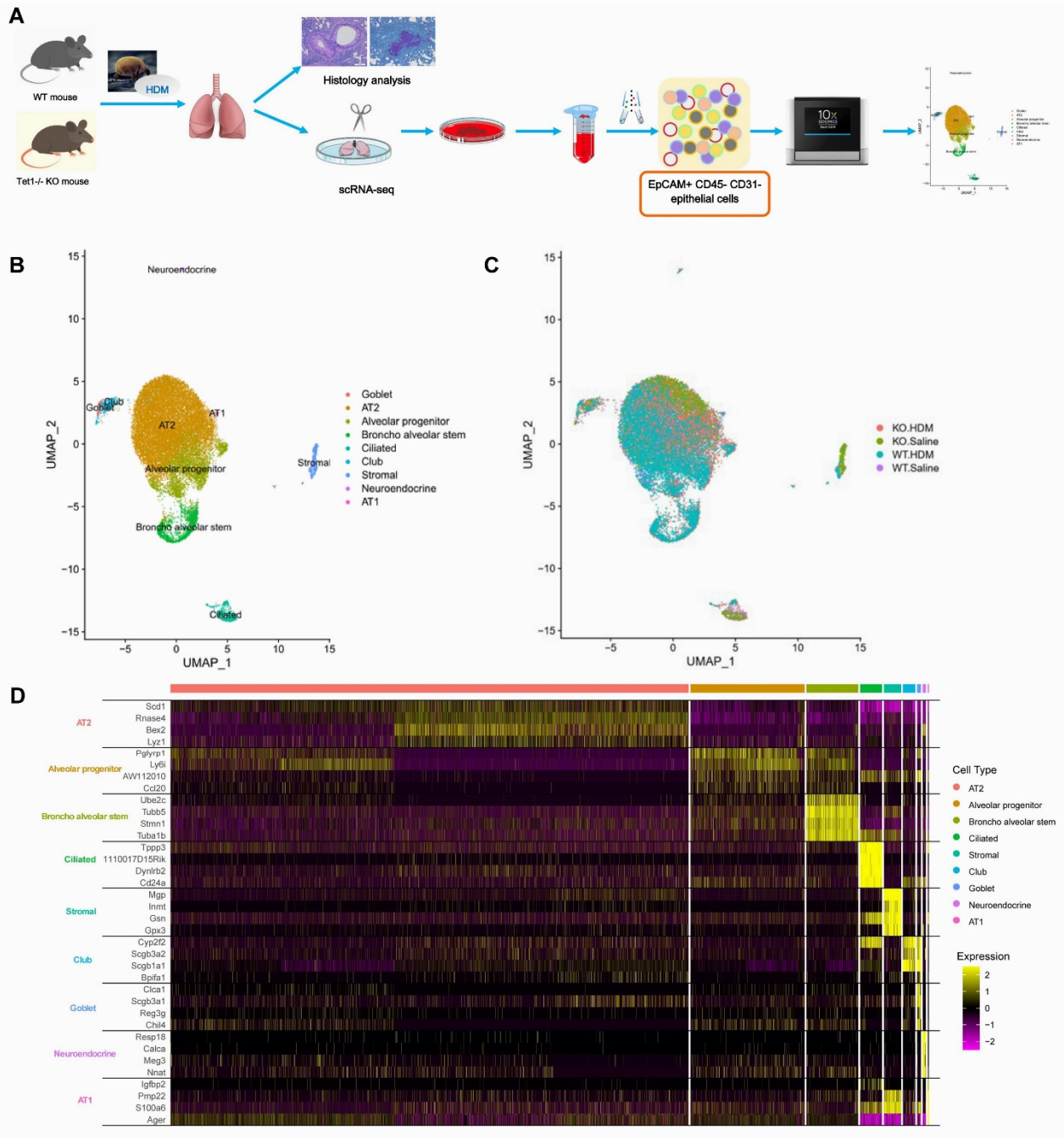

Figure 1. Single-cell RNA sequencing clustering analysis identifies 9 cell types in EpCAM^{+} CD45^{-} CD31^{-} lung cells. (**A**) Schematic overview of the study workflow. (**B**) UMAP visualization of clustering, revealing 9 cell populations. Population identities were determined based on marker gene expression. (**C**) UMAP visualization of EpCAM^{+} CD45^{-} CD31^{-} lung cells in Tet1 KO mice and WT mice with and without HDM challenge. (**D**) Heatmap of top 4 markers in 9 cell clusters.

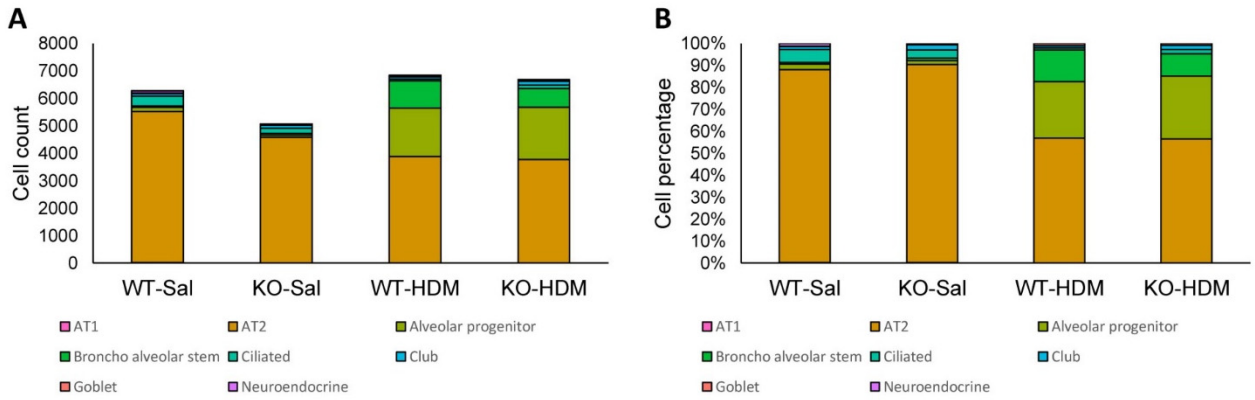

Figure 2. The abundance and percentage of each cell type. (**A**) Abundance of each cell type at each condition; (**B**) percentage of each cell type at each condition.

3.2. Exposure to HDM Led to Cell Type-Specific Changes in the EpCAM$^+$ Lung Epithelial Cells

We identified 830 differentially expressed genes (DEGs) between WT-HDM and WT-Sal cells in our analysis of all EpCAM$^+$ cells (hereafter referred to as bulk cell analysis), regardless of cell type (Table 1 and Table S3). Based on our pathway analysis (IPA) results, several pathways were significantly activated or inhibited, including oxidative phosphorylation (activation z-score = 7.353), sirtuin signaling pathway (z-score = −2.897), and xenobiotic metabolism AHR signaling pathway (z-score = −2.111) (Table S4). We further identified DEGs within each of the eight cell types in the WT-HDM vs. WT-Sal comparison. In total, we found 1773 DEGs within individual cell types (Table 1). All cell types except AT1 had differential expression in the WT-HDM vs. WT-Sal comparison. Of these 1773 DEGs, 616 were unique to one cell type (Figure 3). AT2 cells had the most DEGs associated with HDM treatment (n = 732), followed by AP cells (n = 431) (Table 1 and Table S5). Many genes, including *Il33* [25], *Cxcl5* [26], *Cxcl15* [27], *Ccl20* [28], *Cxcl3* [29], *Cxcl1* [30], *C3* [31], and *Pfn1* [32], which have been linked to asthma pathogenesis, showed a cell type-specific response to HDM (Figure 4A,B, Tables S5 and S6). Subsequently, pathway analysis identified 120 significantly enriched pathways (Table S7). While 98 of these pathways were shared with the bulk cell analysis, 22 pathways were unique to AT2 cells, including ferroptosis signaling pathway, chemokine signaling, and LPS-stimulated MAPK signaling.

Table 1. Number of differential expression genes (DEGs) of EpCAM$^+$ cells.

Comparisons	WT-HDM vs. WT-Sal	KO-Sal vs. WT-Sal	KO-HDM vs. WT-Sal	Overlap of Three Comparisons (Same Direction)	KO-HDM vs. WT-HDM
Bulk cell analysis					
EpCAM+ cells	830	98	817	48 (36)	72
Individual cell types					
AT1	0	0	1	0	0
AT2	732	70	745	39 (30)	78
Alveolar progenitor (AP)	431	18	445	4 (2)	65
Broncho alveolar stem (BAS)	172	4	154	1(1)	51
Ciliated	210	41	200	5 (5)	0
Stromal	72	19	54	0	1
Club	55	5	88	0	0
Goblet	13	0	0	0	0
Neuroendocrine	88	3	16	0	0
Total	1773	160	1703	49 (45)	195

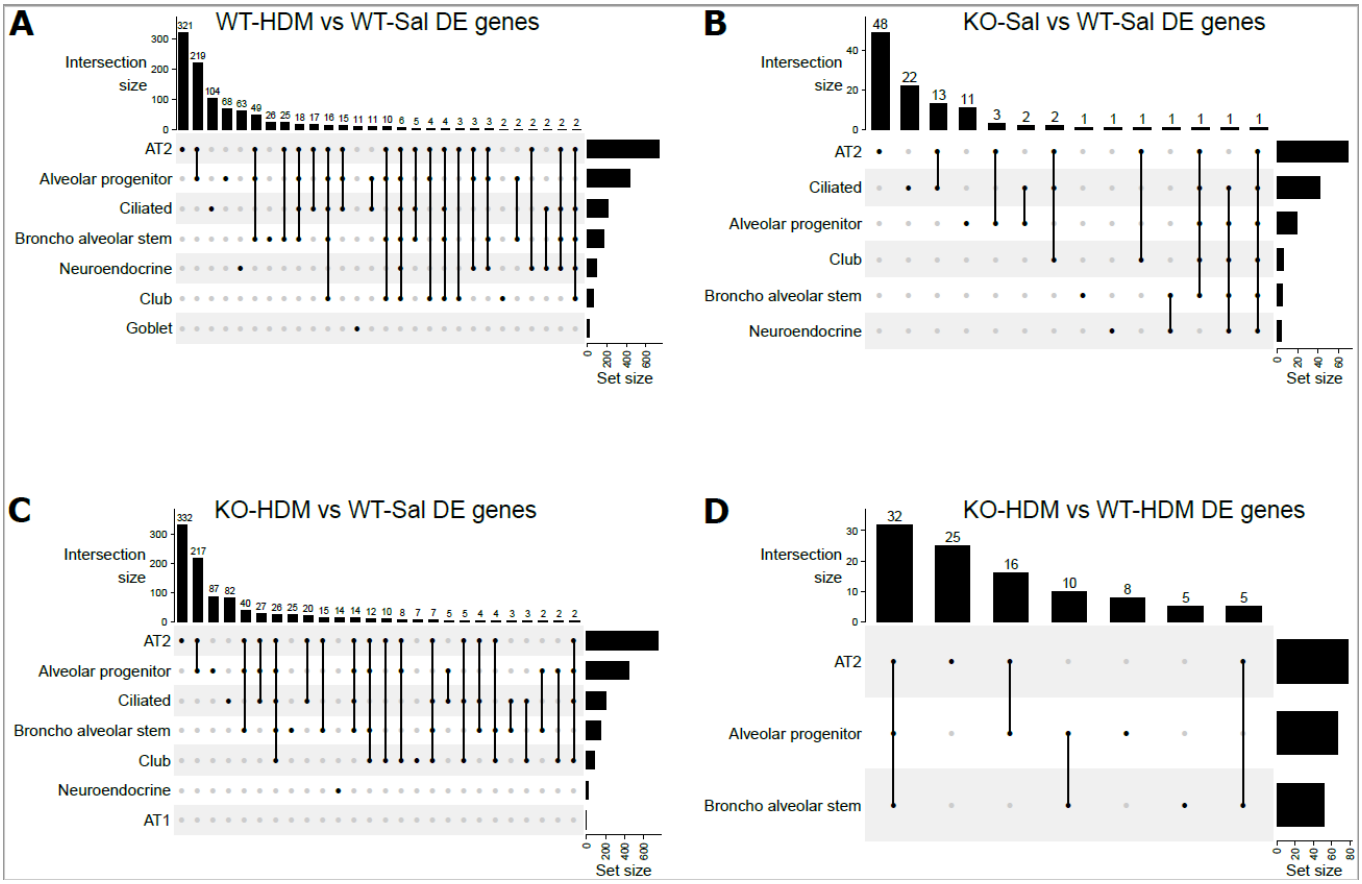

Figure 3. UpSet plots for overlapped DEGs among 8 individual cells types: (**A**) WT-Sal vs. WT-HDM; (**B**) WT-Sal vs. KO-Sal; (**C**) KO-HDM vs. WT-Sal; (**D**) KO-HDM vs. WT-HDM. Dots below vertical bars represent overlapping DEGs among different cell types. Horizontal bars represent the total number of DEGs in each cell type.

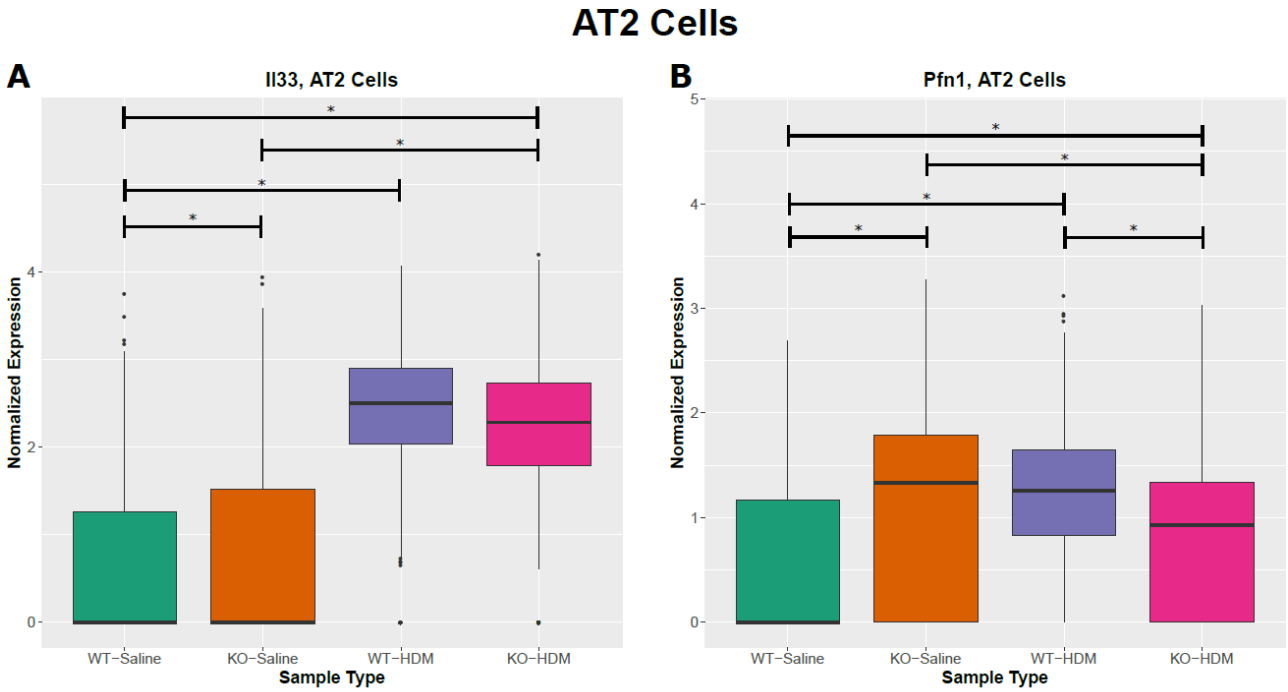

Figure 4. *Cont.*

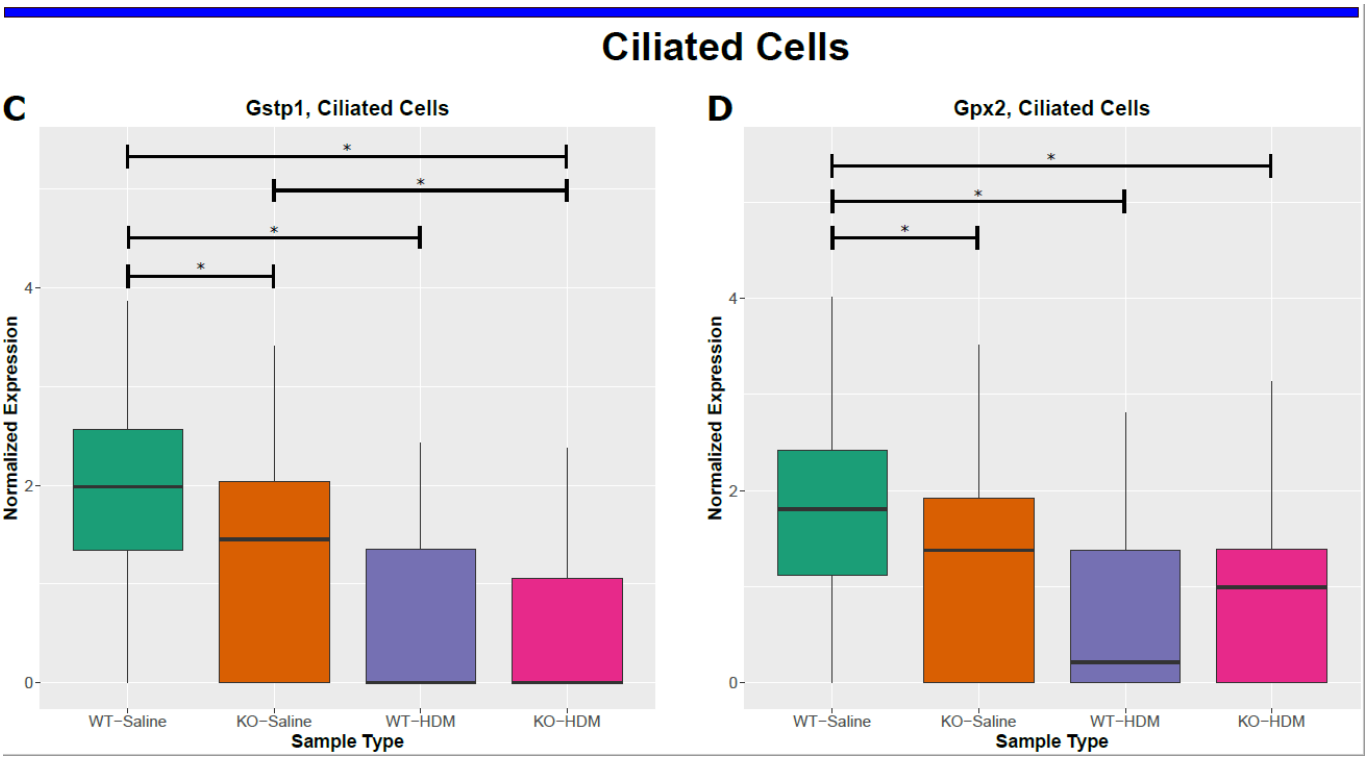

Figure 4. Cell-type specific changes resulting from HDM challenges and/or Tet1 deficiency. (**A**,**B**) AT2 cells; (**C**,**D**) ciliated cells. * represents FDR $\leq$ 0.05.

Ciliated cells are one of the major target cells in asthma [33,34], and injured ciliated cells release inflammatory mediators to aggravate allergen-induced airway inflammation [35,36]. There were 210 DEGs in ciliated cells in the WT-HDM vs. WT-Sal comparison (Figures 3A and 4C,D and Tables S5 and S6). Some DEGs from this comparison, such as *Fos* [37], *Jun* [38], *Hes1* [39], *Cd14* [40], and *C3* [31], have been associated with asthma pathogenesis. Subsequently, we identified 96 significantly enriched pathways in these DEGs (Table S8). NRF2-mediated oxidative stress response was predicted to be inhibited (z-score = −2.333). Furthermore, 18 IPA pathways were enriched in the 104 unique DEGs in ciliated cells, including NRF2-mediated oxidative stress response (Table S8). Collectively, these results suggest that different types of EpCAM$^+$ lung epithelial cells responded to HDM and may contribute to airway inflammation, with common features as well as unique functions.

3.3. Tet1 Knockout Led to Cell-Specific Changes in Baseline EpCAM$^+$ Lung Epithelial Cells

In the bulk cell analysis comparing KO-Sal and WT-Sal cells, 98 genes were differentially expressed (Tables 1 and S3). There were 27 enriched pathways associated with these DEGs (Table S4), including several stress-related pathways (protein ubiquitination pathway/unfolded protein response/eNOS signaling/NRF2-mediated oxidative stress response/glutathione redox reactions I), and pro-inflammatory pathways (interferon signaling/IL-6 signaling/IL-12 signaling and production in macrophages).

Furthermore, we identified Tet1 loss-associated DEGs in each cell type (Tables 1 and S5). AT2 and ciliated cells had the most DEGs. There were 70 such DEGs in AT2 cells, including 48 DEGs unique to AT2 cells (Tables S5 and S6). There were 45 enriched IPA pathways associated with these DEGs (Table S7), including 28 unique to AT2 cells (e.g., AhR signaling/xenobiotic metabolism AHR signaling pathway). Several of these DEGs associated with Tet1 loss in AT2 cells (*Il33* [25], *Areg* [41] and *Bpifa1* [42], *Hspa8* [43] and *Lgals3* [44] (also DEGs in ciliated cells)), have been previously linked to asthma. Additionally, 41 Tet1 loss-associated DEGs were found in ciliated cells (Table 1 and Table S5). Several asthma-

related genes were identified: detoxification enzymes (*Cyp2a5* [45], *Gsto1* [46], *Gstp1* [47], *Gstm1* [48], and *Aldh1a1* [49]) were downregulated while *Hmgb1* (alarmin) [50,51] was upregulated (Figure 4C, Tables S5 and S6). Consistent with our observations following HDM treatment, the downregulation of the detoxification enzymes following Tet1 KO (*Gstp1*, *Gstm1*, and *Gpx2*) were only found in ciliated cells (Figure 4C,D and Table S6). *Hmgb1* was also upregulated in AT2 cells following Tet1 KO. We identified 49 enriched pathways in these DEGs in ciliated cells (Table S8), including a significant inactivation of the xenobiotic metabolism AHR signaling pathway (z-score = −2.449) and an enrichment of several other stress response pathways.

In summary, we found that Tet1 loss in saline-treated mice led to (1) increased expression of alarmins that promote type 2 inflammation, particularly *Il33* (AT2 cells) and *Hmgb1* (AT2 and ciliated cells), (2) the upregulation of genes that promote the proliferation and migration of airway smooth muscle cells and tissue remodeling (*Malat1* (AT2 cells) and *Pfn1* (six cell types)), and (3) the reduced expression of detoxification enzymes (*Gpx2*, *Gstm1*, *Gsto1*, and *Gstp1*) involved in AhR signaling in ciliated cells. Together, this gene dysregulation following Tet1 loss may have resulted in a pro-inflammatory transcriptomic state in AT2 and ciliated cells.

3.4. Tet1 Knockout and HDM Exposure Induced Overlapping Cell Type-Specific Changes in EpCAM$^+$ Lung Epithelial Cells

To further test the hypothesis that the loss of Tet1 generates a proinflammatory transcriptomic state similar to that of HDM, we searched for overlapping genes among the WT-HDM vs. WT-Sal, KO-Sal vs. WT-Sal, and KO-HDM vs. WT-Sal comparisons. In the bulk cell analysis, we identified 48 overlapping DEGs, including 36 DEGs where Tet1 loss and HDM treatment led to changes in the same direction (Table 1 and Table S9). Thirteen of these overlapping DEGs have been linked to asthma, including eight upregulated genes (*Il33, Hmgb1*, *Ager*, *Chia1*, *Ifitm3, Igfbp7*, *Pfn1*, *Retnla*) and five downregulated genes (*Atf3*, *Btg2*, *Klf6*, *Neat1*, and *Sec14l3*) (Figure 4A,B and Figure S3(B1–B12)). Eight mitochondrially encoded genes were also among these thirty-six overlapping DEGs, but their role in asthma is not clear. Next, overlapping DEGs within each cell type were identified and investigated further. In AT2 cells, there were 39 shared DEGs in all 3 different comparisons in AT2 cells (Table S9). Of these 39 DEGs, 30 were affected similarly by Tet1 loss and/or HDM treatment. Meanwhile, there were five different genes that were consistently downregulated in ciliated cells following Tet1 loss and/or HDM treatment (Table S9), including the asthma-associated genes *Gstp1*, *Gstm1*, and *Gpx2* (Figure 4C,D). Additionally, we found that two genes (*Dmkn* and *Chia1*) in AP cells and one gene (*Nnat*) in BAS cells were consistently changed in a similar fashion. Combining all these genes with the same directions of changes in EpCAM+ cells, AT2 cells, AP, BAS, and ciliated cells, there was significant enrichment for NRF2-mediated Oxidative Stress Response, HMGB1 Signaling and Airway Inflammation in Asthma (Table S10). IPA analysis also revealed several significant diseases and functions affected by these overlapping genes, including organ inflammation in EpCAM$^+$ cells and AT2 cells (Figure 5A,B), cell proliferation of fibroblast in AT2 cells (Figure 5C), and the synthesis of reactive oxygen species in ciliated cells (Figure 5D). Collectively, these data support our hypothesis and suggest that the effects of Tet1 knockout in promoting allergen-induced lung inflammation were cell-type dependent.

3.5. Tet1 Dysregulates the Single-Cell Transcriptomic Signature of HDM-Induced Lung Inflammation in Mice

To further understand the effects of Tet1 loss in the presence of HDM, we studied the 72 genes that were differentially expressed in KO-HDM compared with WT-HDM in all EpCAM$^+$ cells (Tables S3 and S6). Among the 72 DEGs, 29 significantly enriched pathways were identified (Table S4), including several stress response pathways and proinflammatory pathways. This is consistent with our previous observations in bulk RNA-seq from the total lungs in mice challenged using the same exposure protocol [9]. Genes involved in tissue injury/repair and remodeling, such as *Areg* [52,53], *Malat1* [54,55], *S100a1* [56,57],

Mt1/2 [58,59], *Scgb1a1* [60,61], and *Clu* [62,63] (Table S3), were upregulated in KO-HDM compared to WT-HDM, even though some of these genes (e.g., *Areg*) were downregulated in KO-Sal mice compared to WT-Sal mice.

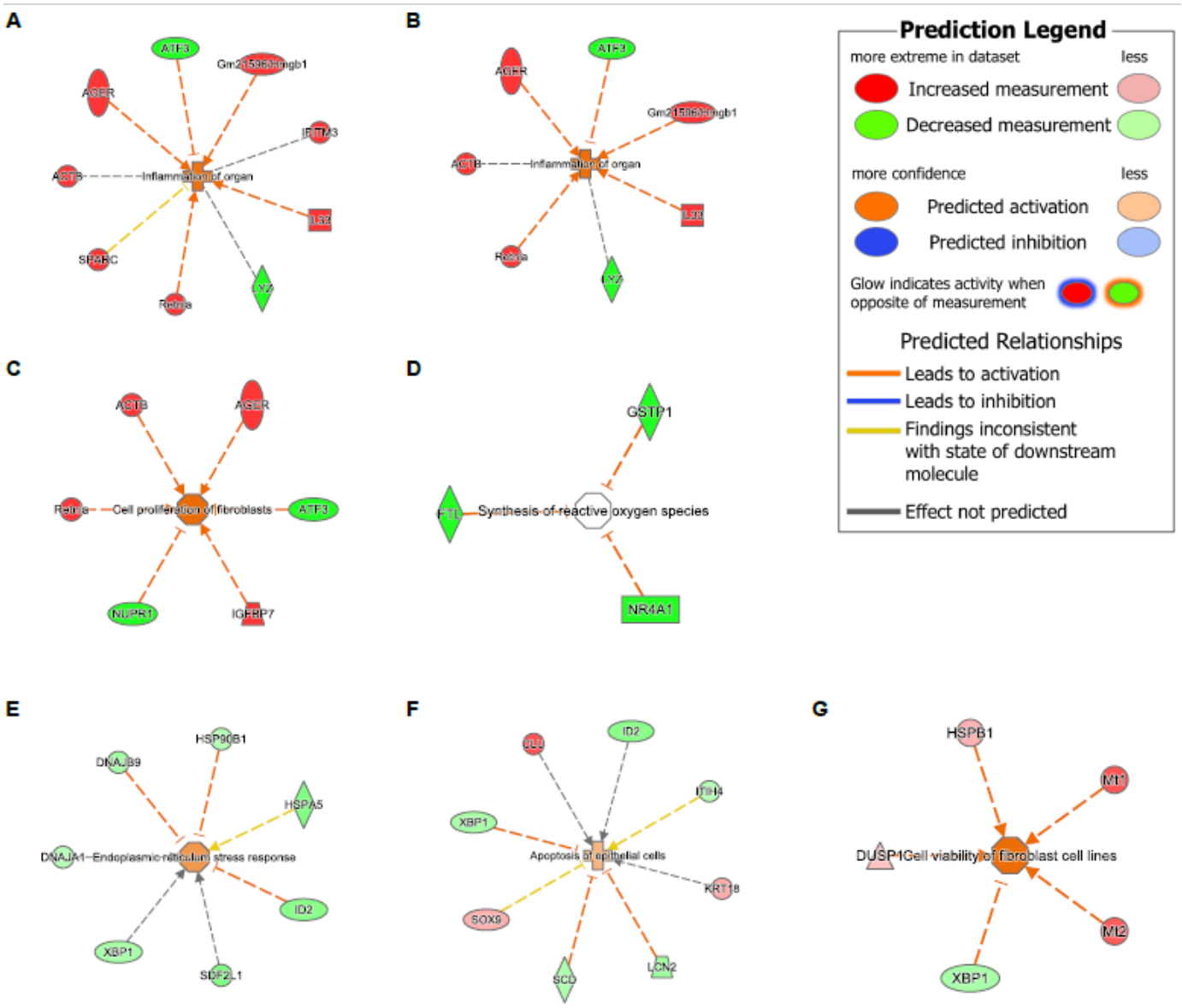

Figure 5. Diseases and function analysis in EpCAM$^+$, AT2, and ciliated cells via IPA. (A-D) DEGs with consistent direction changes among 3 comparisons (WT-HDM vs. WT-Sal, KO-Sal vs. WT-Sal, and KO-HDM vs. WT-Sal). (**A**) Inflammation of organ in EpCAM$^+$ cells (z = 1.866, overlapping $p = 7.54 \times 10^{-4}$). (**B**) Inflammation of organ in AT2 cells (z = 2.097, $p = 2.93 \times 10^{-3}$). (**C**) Cell viability of fibroblast in AT2 cells (z = 2.408, $p = 3.51 \times 10^{-6}$). (**D**) Synthesis of reactive oxygen species in ciliated cells ($p = 3.54 \times 10^{-4}$). (**E**) Endoplasmic reticulum stress response (z = 1.015, $p = 6.74 \times 10^{-6}$), (**F**) apoptosis of epithelial cells (z = 0.651, $p = 6.85 \times 10^{-5}$), and (**G**) cell viability of fibroblast cell lines (z = 2.236, $p = 1.41 \times 10^{-4}$) in DEGs in KO-HDM vs. WT-HDM in AT2 cells.

We then compared KO-HDM with WT-HDM in each cell type. Interestingly, of the 195 DEGs identified across all cell types, 194 were identified in AP cells, AT2 cells, or BAS cells (Table 1 and Figure 3D), and 32 DEGs were shared among all 3 of these cell types. All 32 of these common DEGs changed in the same direction: 16 were upregulated (e.g., *Areg*, *Malat1*, *Mt1/2*, and *Scgb1a1*) and 16 were downregulated (e.g., *Lrg1*, *Pfn1*, and *Rnase4*) in these 3 cell types following Tet1 deletion (Tables S5 and S6). In AT2 cells, specifically, there

were 78 DEGs in KO-HDM compared to WT-HDM, including several genes previously linked to asthma [43,64–66] (Table S6). Further, we identified 32 significantly enriched pathways in the DEGs from AT2 cells (Table S7), including stress response pathways (unfolded protein response/endoplasmic reticulum stress pathway/protein ubiquitination pathway/NRF2-mediated oxidative stress response (gene network shown in Figure 5E), in which most genes showed downregulation in KO-HDM. Not surprisingly, the same pathways were also significantly enriched among combined DEGs from all EpCAM$^+$ cells, AT2 cells, AP, and BAS with the same directions of changes in the KO-HDM vs. WT-HDM comparison (Table S11). Genes involved in apoptosis and cell viability were also found (Figure 5F,G). Similar to the bulk cell analysis, several chemokines and cytokines (e.g., *Cxcl5*) showed reduced expression in KO-HDM (Table S6). In summary, our data suggest that, following HDM challenges, the loss of Tet1 led to the downregulation of genes in stress response pathways, potentially leading to cell apoptosis, tissue injury, and additional lung inflammation and remodeling.

3.6. Tet1 Knockout and HDM Exposure Induced Cell Type-Specific Changes in Transcription Factor (TF) Activity in EpCAM$^+$ Lung Epithelial Cells

As Tet1 may regulate gene expression through interacting with TFs, TF activity in individual cell types was explored using DoRothEA [20–22]. Consistent with previous findings [67–69], we observed cell type-specific TF activity, consistent with their cell type-specific regulation of gene expression programs (Figure 6A). For example, *E2f1-4* and *Tfdp1* (both promote the expression of a cell cycle-related network [67]) were highly activated in BAS compared to all other cell types, while the activities of *Rest* (a repressor of neuronal genes in non-neuronal cells [70]) and *Rreb1* were lowest in neuroendocrine cells. Additionally, there was relatively high activity of *Rfx1* (promotes ciliogenesis [71,72]) in ciliated cells. Because AT2 cells were the most abundant cell type, there were generally only small changes in TFs activity compared to the average across all cells in our heatmap (Figure 6A). However, a group of TFs, including *Foxa1*, *Sox10*, and *Runx2*, showed relatively high activity levels in AT2 cells, and these TFs are essential in conducting airway and alveolar epithelium development and repair [73–75].

We also found that TF activity levels were altered by HDM and Tet1 loss in individual cell types, such as AT2 cells (Figure 6B–E) and ciliated cells (Figure 6F–H). For example, regardless of Tet1 status, *Foxa1* (also decreased in expression in HDM samples in AT2 cells, Table S5) and *Hnf1a* activities were reduced by HDM in AT2 cells (Figure 6B), while the activities of *Rest, Rreb1*, and *Nr2c2* were increased by HDM in both AT2 and ciliated cells (Figure 6B,F). Meanwhile, *Smad3*, *Smad4*, and *Sp3* activities were decreased by HDM in ciliated cells (Figure 6F). When looking specifically for effects of Tet1, we found that the activities of *Myc, Rest*, and *Rreb1* were consistently reduced when Tet1 was lost in AT2 cells, regardless of HDM status (Figure 6C). Hif1α, whose expression is regulated by Tet1 [76] and may also regulate Tet1 expression during oxidative stress [77], showed reduced activity in KO-Saline (Figure 6D). Increased *Foxa1* activity was only observed in KO-HDM compared to WT-HDM (Figure 6E). In ciliated cells, however, nearly all effects of Tet1 loss were specific to the treatment state (Figure 6F). With saline treatment, activities of *Nfe2l2* (encoding Nrf2), *Nfe2l1* (encoding Nrf1) and their binding partner Mafk (Figure 6G) [78] were reduced in Tet1 KO cells compared to wild-type cells; these TFs are involved in various stress responses, including oxidative stress [79,80], and regulate the expression of ROS-detoxifying enzymes including *Gstp1*, *Gstm1*, and *Gpx2* [81]. Meanwhile, TFs involved in the aryl hydrocarbon receptor signaling pathway (AhR) and the TGFβ signaling pathway (Smad3, Smad4) had higher activity in KO-HDM compared to WT-HDM, even though HDM challenges reduced their activity (Figure 6F,H). Collectively, our data suggest that TFs respond to HDM challenges and Tet1 loss in a cell type-specific manner, which may contribute to cell type-specific transcriptomic changes that could be associated with lung inflammation.

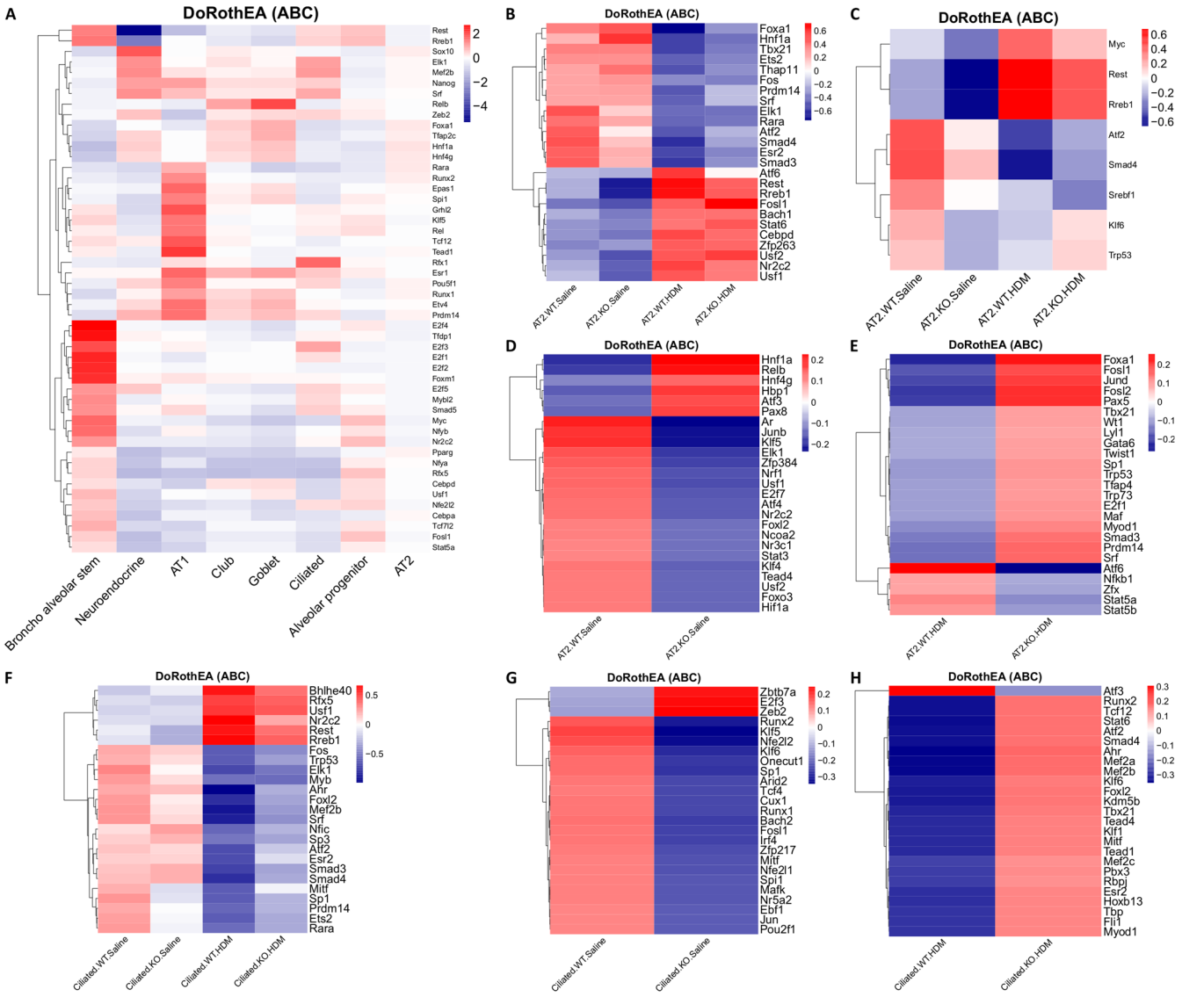

Figure 6. Heatmaps of transcription factor (TFs) activities analyzed using DoRothEA. (**A**) Top 50 most variable TFs by gene activity across 8 individual cell types. (**B**) Top 25 TFs across all AT2 cells. (**C**) TFs that were in the top 25 in both the KO-HDM vs. WT-HDM and KO-Saline vs. WT-Saline comparisons in AT2 cells. (**D**) Top 25 TFs in the KO-Saline vs. WT-Saline comparison that were not in the top 25 for KO-HDM vs. WT-HDM in AT2 cells. (**E**) Top 25 TFs in the KO-HDM vs. WT-HDM comparison that were not in the top 25 for KO-Saline vs. WT-Saline in AT2 cells. (**F**) Top 25 most-variable TFs in ciliated cells. (**G**) Top 25 most-variable TFs in ciliated cells in KO-Saline vs. WT-Saline. (**H**) Top 25 most-variable TFs in ciliated cells in KO-HDM vs. WT-HDM.

3.7. HDM, Not Tet1, Promotes the Differentiation of AP and BAS Cells into AT2 Cells

As observed above, HDM challenges seemingly reduced AT2 cell proportions and increased AP and BAS cell proportions (Figure 2 and Table S2). It has been established that AT2 cells can differentiate from AP and BAS cells [82,83]. Therefore, we performed single-cell trajectory analysis to explore the roles of HDM and/or Tet1 KO in AT2 cell differentiation (Figures S4 and S5). Initially, AT2, AP, and BAS cells from all groups were combined (Figure S4A), and then cell fates were separated at branch point 4 (Figure S4B). Our data support that AT2 cells differentiated from AP and BAS cells. Comparing WT-HDM to WT-Sal and KO-HDM to KO-Sal, HDM-challenged cells were clearly separated along the trajectory from saline-treated cells, indicating that HDM promotes AP and BAS proliferation (Figure S4C–H). However, this was not observed in the KO-Sal vs. WT-Sal

comparison, as no clear branch point was identified to separate cell fates, indicating that Tet1 KO did not have a substantial impact on AP and BAS proliferation (Figure S4I–K). Thus, heatmaps showing significant changes along the trajectory were only generated for the other comparisons (Figure S5). *Sftpc* (a marker for AT2 and BAS cells), *Sftpa1* (a marker for AT2 and AP cells), and *Sftpb* (a marker for only AT2 cells) varied significantly along all trajectories, other than in the saline-only comparison (there were no comparable genes for this comparison due to a lack of clear branch points separating cell fates; Table S1, Figure S5). Combined with evidence in Figure S4 and Table S2, these results suggest that HDM-induced AT2 cell injury promoted the proliferation and differentiation of AP and BAS cells. Tet1 knockout did not appear to affect the differentiation of AP and BAS cells into AT2 cells.

4. Discussion

The lung is an organ with continuous exposure to environmental challenges, such as allergens and pathogens. The epithelium is the first line of defense for the lung. Lung epithelium (airway epithelium [84] and alveolar epithelium [85,86]) injury and inflammation play critical roles in asthma. Our previous study [9] found that Tet1 deletion enhanced HDM-induced lung inflammation in mice, and that it was linked to transcriptomic changes in proinflammatory molecules (*Il33*) and detoxification enzymes (*Gsto1* and *Aldh1a1*) in total lung RNA. Furthermore, our previous results indicated that 59 pathways, including NRF2-mediated oxidative stress response, AhR signaling, and the interferon (IFN) signaling pathway, were significantly altered. However, the effects of Tet1 loss in specific lung cell types and the contribution of individual cell types in HDM-induced transcriptomic alterations remained unknown. Data from our current analyses showed that while AT2, alveolar progenitor cells, broncho alveolar stem cells, and ciliated cells underwent transcriptional changes following HDM challenges, AT2 and ciliated cells were the cell types most affected by Tet1 loss. Following HDM treatment, the upregulation of the alarms *IL33* and *Hmgb1* mainly occurred in AT2 cells, while the downregulation of detoxification enzymes mainly occurred in ciliated cells. Notably, Tet1 knockout had similar effects on alarms in AT2 cells and detoxification enzymes in ciliated cells. Further, in the presence of HDM, we found that genes involved in stress response pathways (e.g., *Xbp1*, *Dnajb9*, and *Hspa8*) and markers for tissue damage response/remodeling (e.g., *Clu*, *Mt1/2*) were upregulated. Based on these observations, a model linking Tet1 loss to increased airway inflammation was proposed (Figure 7). Although this model warrants further validations to establish the direct contributions of these pathways to Tet1-mediated inflammation, our data provide supporting evidence at the transcriptomic level. Future studies focusing on mechanisms through which Tet1 regulates these genes in the lung epithelium would also provide clarity on the regulatory process.

Some genes that were differentially expressed in our previous bulk RNA-seq analyses were not found in the current scRNA-seq analyses, and vice versa. It is possible that HDM-induced transcriptomic changes masked the effects of Tet1 knockout on lung epithelial cells in our current study. Meanwhile, increased noise in scRNA-seq data, lower power due to small cell numbers, the differences in how DEGs were defined in the scRNA-seq dataset compared to our previous RNA-seq studies, and the possible contribution of other lung non-epithelial cell types in bulk RNA-seq were also potential reasons for these inconsistencies. On a related note, in our current study, we observed the downregulation of several asthma-associated genes (e.g., *Cxcl5, Atf3* [87], and *Btg2* [88]) that are normally increased by HDM challenges, possibly due to the time-dependent expression pattern of these molecules during the acute phase of inflammation; this needs further investigation. In general, however, we noted a differential expression of several candidate genes in our scRNA-seq dataset that was consistent with prior studies. These include genes involved in oxidative stress responses and AhR signaling/detoxification, pro-inflammatory responses and alarmins, and tissue damage and repair, many of which are known to contribute to airway inflammation in asthma.

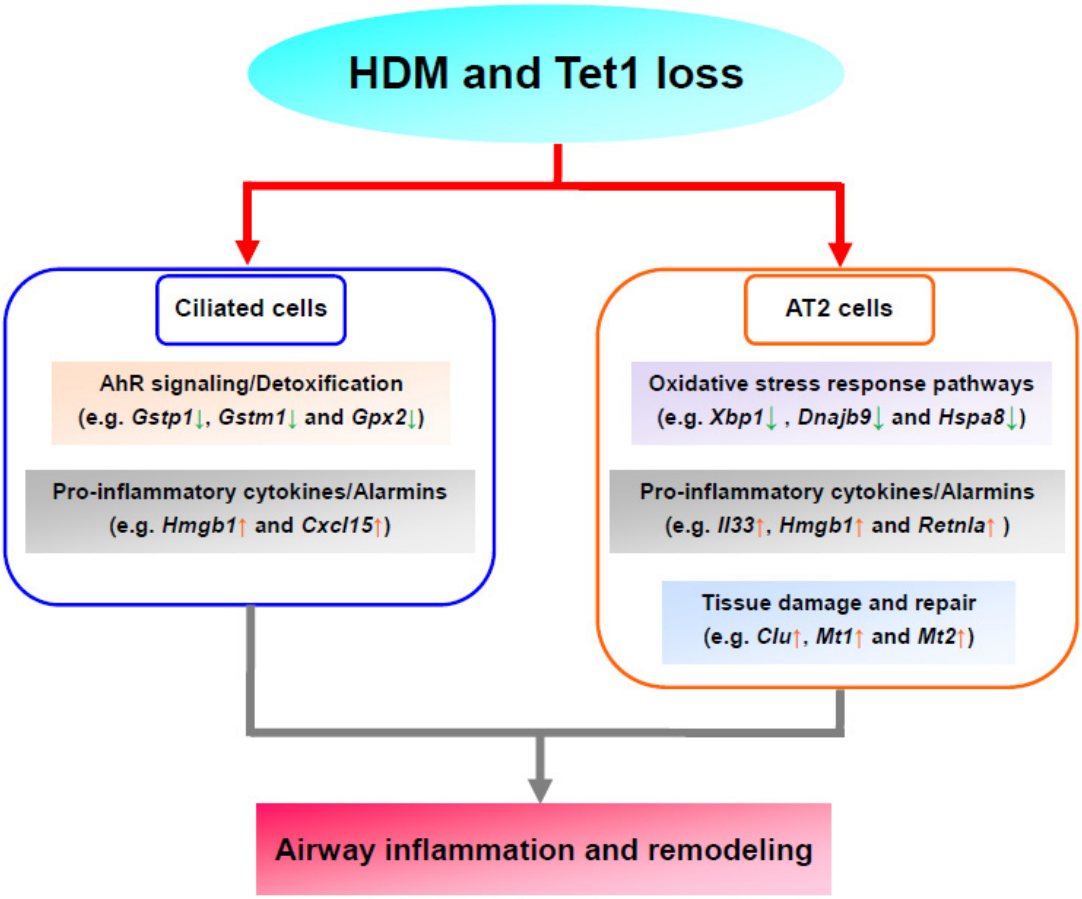

Figure 7. Proposed model based on transcriptomic analysis. Tet1 deletion downregulated (downward arrows in green) genes in AhR signaling/detoxification (ciliated cells, base line) and oxidative stress responses (AT2 cells, with HDM), and upregulated (upward arrows in red) genes in pro-inflammatory cytokines/alarmins (AT2 and ciliated cells, baseline) and tissue damage and repair (AT2 cells, with HDM). Collectively, this may aggravate HDM-induced airway inflammation and remodeling.

AT2 cells were the most abundant cell type in our dataset (69.7% in total). Although no significant pathological alterations in alveoli were observed in either asthmatic patients or animal models, several studies [85,86,89] have reported that AT2 cells are a major contributor of inflammatory mediators in asthma. In particular, Ravanetti L. et al. supported that AT2 cells are one major source of IL-33 in mice with HDM-induced lung inflammation [89]. Our present study supports that HDM may enhance AT2 cell differentiation from AP and BAS cells (Figure S4), likely due to HDM-induced AT2 cell injury and death (Figure 2 and Table S2). Our cell type-specific transcriptomic analysis showed that AT2 cells were one major source of inflammatory mediators and molecules, especially *Il33* (Figure 4A), *Hmgb1*, *Ager* (Figure S3(A1)), and *Retnla* (Figure S3(A2)), in allergen-induced lung inflammation (Table S6). Allergens may induce lung Th2 inflammation through AT2 cell injury, which releases alarms such as *Il33* [25] and *Hmgb1* [90], and Tet1 plays a critical role in this process by regulating their expression. Additionally, when comparing KO-HDM to WT-HDM in AT2 cells, we found that tissue damage and repair genes were upregulated, while oxidative stress response genes were downregulated; most of these genes were also DEGs in all EpCAM$^+$ cells (Table S6). The downregulation of oxidative stress response pathways, especially unfolded protein response (UPR), may result in apoptosis and cell death [91], and the roles of UPR in oxidative stress response, cytokine production, and asthma pathogenesis are emerging [92]. Taken together, our data suggest that while AT2 cells from Tet1 knockout mice at baseline have a pro-inflammatory transcriptomic signature (elevated alarms and

reduced detoxification enzymes), HDM challenges may further induce cell damage and death due to elevated oxidative stress and downregulated stress responses.

Ciliated cells are another major cell type within airway epithelium. Ciliated cells are essential for mucociliary clearance through their motile cilia's coordinated directional movement, and can sense and respond to allergens, air pollution particles, and pathogens [33,93]. Asthma can cause cilia dysfunction and ultrastructural abnormalities, such as the decrease of ciliary beat frequency, the generation of dyskinetic and immotile cilia, and the disruption of tight junctions, which were closely associated with asthma severity [94]. Meanwhile, multiple studies [36,95] suggest that ciliated cells are a source of cytokines, such as IL33 and TSLP, in asthma. In our single-cell analysis, we only observed a trend of increase for *Il33* at baseline when Tet1 was deficient, and no further changes following HDM treatment. However, in vitro studies using HBECs showed that the loss of Tet1 significantly increased *IL33* expression following 24 h of HDM challenges (Supplementary Figure S6), which support that Tet1 deficiency promotes the predisposition of allergic inflammation in ciliated cells. Further, we found that *Gstp1*, *Gstm1*, and *Gpx2* were all downregulated with HDM and/or Tet1 loss in ciliated cells (Figure 4C,D). These three genes (along with two others: *Ftl1* and *Nr4a1*) were consistently downregulated in ciliated cells, but not in AT2 cells (Table S9), implying that there were unique responses to Tet1 loss and HDM treatment in ciliated cells. Our previous studies in HBECs showed that Tet1 regulates detoxification enzymes in HEBCs as well [9]. Together, these data highlight the unique role of ciliated cells and suggest that Tet1 may regulate HDM-induced lung inflammation via the regulation of AhR signaling/detoxification and pro-inflammatory cytokines/alarmins in ciliated cells (Figure 7).

Our data also suggest that HDM and/or Tet1 KO in mice lungs led to cell type-specific changes in TF activity levels (Figure 6). Our prior study using HBECs suggested that Tet1 protects against HDM-induced allergic inflammation at least partially by regulating the AhR pathway [9]. Data from the current study in ciliated cells support that AhR activity and the AhR pathway were altered following Tet1 KO and/or HDM treatment (Figure 6F,H and Figure 7). Meanwhile, Nrf1/2 activity was lower in KO-Saline mice, compared to WT-Saline (Figure 6G), which may explain the lower expression of *Gstp1*, *Gstm1*, and *Gpx2* in KO-Sal, compared to WT-Sal, as the Nrf2-mediated pathway is an alternative to the AhR pathway that regulates the expression of antioxidant enzymes [81]. In addition, consistent with an increased expression of markers for tissue damage and repair, the activity of Foxa1, a TF essential in airway epithelium development [96] and barrier integrity [75], was increased in KO-HDM compared to WT-HDM. Of note, these activity levels for the transcription factors were estimated using gene expression profiles of their targets, not the direct expressions of the transcription factor themselves. Even if the direct expression of a transcription factor were not altered, it is possible that Tet1 KO or HDM treatment could alter transcription factor activities, especially considering that Tet1 can directly interact with transcription factors [97,98]. Taken together, these results indicate that Tet1 plays an important role in regulating TF activity that may directly impact allergen-induced lung inflammation.

5. Conclusions

Collectively, our results revealed possible mechanisms underlying the protective role of Tet1 in HDM-induced lung inflammation at the single-cell level. Different epithelial cells played common and unique roles in allergic lung responses. The major cellular contributors of multiple asthma-associated inflammatory mediators, such as *Il33*, *Hmgb1*, *Retnla*, and *Ager* were identified, and a cluster of novel allergy-associated molecules, such as *Chia1*, *Nnat*, and *Nr4a1* were found in different lung epithelial cells. Future studies should attempt to elucidate the role of these novel targets in asthma. Our results suggest that AT2 cells are essential for Th2 inflammation through stress responses, alarms, tissue injury and repair in allergen-induced lung inflammation, and that these genes are regulated by Tet1. In ciliated cells, Tet1 promotes the Xenobiotic Metabolism AhR signaling pathway, especially the detoxification enzymes, which may protect the lung from allergen-induced

inflammation. As chronic airway inflammation induced by allergens plays a critical role in the pathophysiology of asthma, these novel findings support that Tet1 is a potential therapeutic target of asthma.

Supplementary Materials: The following supporting information can be downloaded at: https://www.mdpi.com/article/10.3390/genes13050880/s1, Supplementary Figure S1: (A) Treatment Protocol; (B) Lung epithelial cells ($CD326^+$ $CD31^-$ $CD45^-$ cells) sorting. Representative sorting images (one from WT and one from KO are shown); (C) and (D) Lung pathological alterations and airway mucus secretion in HDM-induced airway inflammation in mice. [(C) HE staining. The figure demonstrates a representative view (×200) from each group. (D) PAS staining. The figure demonstrates a representative view (×200) from each group.]. Supplementary Figure S2: Cell type-specific expression of *Epcam* and *Scgb1a1*. Boxplots showing the expression levels of (A) *Epcam*, (B) *Scgb1a1* and (c) *Tet1* for each epithelial cell type. Supplementary Figure S3. The expressions of asthma-associated DEGs (WT-Sal vs WT-HDM, WT-Sal vs KO-Sal, and KO-HDM vs WT-Sal overlapped DEGs) in (A1-10) AT2 cells, (B1-12) $EpCAM^+$ lung epithelial cells, and (C1-2) ciliated cells. Supplementary Figure S4. Single-cell trajectory analysis reveals the differentiation of AP and BAS cells into AT2 cells. Supplementary Figure S5. Expression heatmap of dynamically expressed genes ordered across single-cell trajectory analysis reveals the differentiation of AP cells and BAS into AT2 cells. Supplementary Figure S6. Impact of TET1 knockdown and HDM treatment in *IL33* expression in HBECs. (A) TET1. (B) IL33. Supplementary Table S1. Markers used to define all the cell types. Supplementary Table S2. Cell number in each group identified by scRNA-seq analysis. Supplementary Table S3. Differentially expressed genes (DEGs) from bulk analysis (all $EpCAM^+$ cells). Supplementary Table S4. Enriched pathways with DEGs from bulk analysis by IPA analysis. Supplementary Table S5. Differentially expressed genes from each cell type. Supplementary Table S6. Examples of cell type-specific changes induced by HDM challenges and Tet1 loss. Supplementary Table S7. Enriched pathways with AT2-specific DEGs by IPA analysis. Supplementary Table S8. Enriched pathways with ciliated cell-specific DEGs by IPA analysis. Supplementary Table S9. Genes with the same directions of changes among WT-HDM vsWT-Sal, KO-SalvsWT-Sal, and KO-HDMvsWT-Sal. Supplementary Table S10 Enriched pathways within genes with the same directions of changes among WT-HDM vs WT-Sal, KO-Sal vs WT-Sal, and KO-HDM vs WT-Sal in all $EpCAM^+$ cells, AT2 cells, AP, BAS, and ciliated cells. Supplementary Table S11. Enriched pathways within combined DEGs from all $EpCAM^+$ cells, AT2 cells, AP, and BAS with the same directions of changes in KO-HDMvsWT-HDM.

Author Contributions: H.J. conceived the study. T.Z. drafted the manuscript with the help of A.P.B. and H.J. T.Z. established and characterized the mouse model with the help of L.P.C. A.P.B. performed scRNA-seq data processing and analysis. L.P.C. performed sample processing and assisted in library preparation. G.Q. assisted in scRNA-seq data processing and provided input in cell clustering. All authors have read and agreed to the published version of the manuscript. Part of this study has been published as an abstract (https://doi.org/10.1164/ajrccm-conference.2019.199.1_MeetingAbstracts.A604, https://doi.org/10.1164/ajrccm-conference.2020.201.1_MeetingAbstracts.A7402, and https://doi.org/10.1016/j.jaci.2021.12.270).

Funding: This research was supported by NIH/NIAID R01AI141569-1A1 (to H.J.). H.J. was also supported by NIH/NIEHS P30ES023513-supported EHSC scholar fund and UC Davis Faculty Startup fund. Funding was also provided by NSF CAREER award 1846559 to G.Q.

Institutional Review Board Statement: The study was conducted in accordance with the Declaration of Helsinki, and approved by the Institutional Animal Care and Use Committee at University of California Davis (protocol code 20972 approved on 28 February 2019).

Informed Consent Statement: Not applicable.

Data Availability Statement: The data have been deposited to the NCBI Sequence Read Archive (SRA), accession # PRJNA838071.

Conflicts of Interest: The authors declare no conflict of interest.

References

1. Scherzer, R.; Grayson, M.H. Heterogeneity and the origins of asthma. *Ann. Allergy Asthma Immunol.* **2018**, *121*, 400–405. [CrossRef]
2. Xu, C.-J.; Söderhäll, C.; Bustamante, M.; Baïz, N.; Gruzieva, O.; Gehring, U.; Mason, D.; Chatzi, L.; Basterrechea, M.; Llop, S.; et al. DNA methylation in childhood asthma: An epigenome-wide meta-analysis. *Lancet Respir. Med.* **2018**, *6*, 379–388. [CrossRef]
3. Lee, Y.; Hwang, Y.-H.; Kim, K.-J.; Park, A.-K.; Paik, M.-J.; Kim, S.H.; Lee, S.U.; Yee, S.-T.; Son, Y.-J. Proteomic and transcriptomic analysis of lung tissue in OVA-challenged mice. *Arch. Pharmacal Res.* **2018**, *41*, 87–100. [CrossRef]
4. Cui, J.; Lv, Z.; Teng, F.; Yi, L.; Tang, W.; Wang, W.; Tulake, W.; Qin, J.; Zhu, X.; Wei, Y.; et al. RNA-Seq Expression Analysis of Chronic Asthmatic Mice with Bu-Shen-Yi-Qi Formula Treatment and Prediction of Regulated Gene Targets of Anti-Airway Remodeling. *Evid. -Based Complement. Altern. Med.* **2021**, *2021*, 1–9. [CrossRef]
5. Zhu, T.; Zhang, X.; Chen, X.; Brown, A.P.; Weirauch, M.T.; Guilbert, T.W.; Hershey, G.K.K.; Biagini, J.M.; Ji, H. Nasal DNA methylation differentiates severe from non-severe asthma in African-American children. *Allergy* **2021**, *76*, 1836–1845. [CrossRef]
6. Forno, E.; Wang, T.; Qi, C.; Yan, Q.; Xu, C.-J.; Boutaoui, N.; Han, Y.-Y.; Weeks, D.; Jiang, Y.; Rosser, F.; et al. DNA methylation in nasal epithelium, atopy, and atopic asthma in children: A genome-wide study. *Lancet Respir. Med.* **2019**, *7*, 336–346. [CrossRef]
7. Qi, C.; Jiang, Y.; Yang, I.V.; Forno, E.; Wang, T.; Vonk, J.M.; Gehring, U.; Smit, H.A.; Milanzi, E.; Carpaij, O.A.; et al. Nasal DNA methylation profiling of asthma and rhinitis. *J. Allergy Clin. Immunol.* **2020**, *145*, 1655–1663. [CrossRef]
8. Yu, Q.; Zhou, B.; Zhang, Y.; Nguyen, E.T.; Du, J.; Glosson, N.L.; Kaplan, M.H. DNA methyltransferase 3a limits the expression of interleukin-13 in T helper 2 cells and allergic airway inflammation. *Proc. Natl. Acad. Sci. USA* **2012**, *109*, 541–546. [CrossRef]
9. Burleson, J.D.; Siniard, D.; Yadagiri, V.K.; Chen, X.; Weirauch, M.T.; Ruff, B.P.; Brandt, E.; Hershey, G.K.K.; Ji, H. TET1 contributes to allergic airway inflammation and regulates interferon and aryl hydrocarbon receptor signaling pathways in bronchial epithelial cells. *Sci. Rep.* **2019**, *9*, 7361. [CrossRef]
10. Zhang, X.; Chen, X.; Weirauch, M.T.; Zhang, X.; Burleson, J.D.; Brandt, E.; Ji, H. Diesel exhaust and house dust mite allergen lead to common changes in the airway methylome and hydroxymethylome. *Environ. Epigenetics* **2018**, *4*, dvy020. [CrossRef]
11. Somineni, H.K.; Zhang, X.; Biagini Myers, J.M.; Kovacic, M.B.; Ulm, A.; Jurcak, N.; Ryan, P.H.; Hershey, G.; Ji, H. Ten-eleven translocation 1 (TET1) methylation is associated with childhood asthma and traffic-related air pollution. *J. Allergy Clin. Immunol.* **2016**, *137*, 797.e795–805.e795. [CrossRef]
12. Zhu, T.; Brown, A.P.; Ji, H. The Emerging Role of Ten-Eleven Translocation 1 in Epigenetic Responses to Environmental Exposures. *Epigenetics Insights* **2020**, *13*, 2516865720910155. [CrossRef]
13. Zheng, G.X.Y.; Terry, J.M.; Belgrader, P.; Pyvkin, P.; Bent, Z.W.; Wilson, R.; Ziraldo, S.B.; Wheeler, T.D.; McDermott, G.P.; Zhu, J.; et al. Massively parallel digital transcriptional profiling of single cells. *Nat. Commun.* **2017**, *8*, 14049. [CrossRef]
14. Stuart, T.; Butler, A.; Hoffman, P.; Hafemeister, C.; Papalexi, E.; Mauck, W.M., III; Hao, Y.; Stoeckius, M.; Smibert, P.; Satija, R. Comprehensive Integration of Single-Cell Data. *Cell* **2019**, *177*, 1888.E21–1902.E21. [CrossRef]
15. Miettinen, M.; Lindenmayer, A.E.; Chaubal, A. Endothelial cell markers CD31, CD34, and BNH9 antibody to H- and Y-antigens—Evaluation of their specificity and sensitivity in the diagnosis of vascular tumors and comparison with von Willebrand factor. *Mod. Pathol.* **1994**, *7*, 82–90.
16. Scialdone, A.; Natarajan, K.N.; Saraiva, L.; Proserpio, V.; Teichmann, S.; Stegle, O.; Marioni, J.C.; Buettner, F. Computational assignment of cell-cycle stage from single-cell transcriptome data. *Methods* **2015**, *85*, 54–61. [CrossRef]
17. Johansen, N.; Quon, G. scAlign: A tool for alignment, integration, and rare cell identification from scRNA-seq data. *Genome Biol.* **2019**, *20*, 166. [CrossRef]
18. Han, X.; Wang, R.; Zhou, Y.; Fei, L.; Sun, H.; Lai, S.; Saadatpour, A.; Zhou, Z.; Chen, H.; Ye, F.; et al. Mapping the Mouse Cell Atlas by Microwell-Seq. *Cell* **2018**, *172*, 1091.e17–1107.e17. [CrossRef]
19. Schilders, K.A.A.; Eenjes, E.; Van Riet, S.; Poot, A.A.; Stamatialis, D.; Truckenmüller, R.; Hiemstra, P.S.; Rottier, R.J. Regeneration of the lung: Lung stem cells and the development of lung mimicking devices. *Respir. Res.* **2016**, *17*, 44. [CrossRef]
20. Garcia-Alonso, L.; Holland, C.H.; Ibrahim, M.M.; Turei, D.; Saez-Rodriguez, J. Benchmark and integration of resources for the estimation of human transcription factor activities. *Genome Res.* **2019**, *29*, 1363–1375. [CrossRef]
21. Holland, C.H.; Szalai, B.; Saez-Rodriguez, J. Transfer of regulatory knowledge from human to mouse for functional genomics analysis. *Biochim. Biophys. Acta Gene Regul Mech.* **2019**, *1863*, 194431. [CrossRef] [PubMed]
22. Holland, C.H.; Tanevski, J.; Perales-Patón, J.; Gleixner, J.; Kumar, M.P.; Mereu, E.; Joughin, B.A.; Stegle, O.; Lauffenburger, D.A.; Heyn, H.; et al. Robustness and applicability of transcription factor and pathway analysis tools on single-cell RNA-seq data. *Genome Biol.* **2020**, *21*, 1–19. [CrossRef] [PubMed]
23. Alvarez, M.J.; Shen, Y.; Giorgi, F.M.; Lachmann, A.; Ding, B.B.; Ye, B.H.; Califano, A. Functional characterization of somatic mutations in cancer using network-based inference of protein activity. *Nat. Genet.* **2016**, *48*, 838–847. [CrossRef]
24. Trapnell, C.; Cacchiarelli, D.; Grimsby, J.; Pokharel, P.; Li, S.; A Morse, M.; Lennon, N.J.; Livak, K.J.; Mikkelsen, T.S.; Rinn, J.L. The dynamics and regulators of cell fate decisions are revealed by pseudotemporal ordering of single cells. *Nat. Biotechnol.* **2014**, *32*, 381–386. [CrossRef]
25. Hong, H.; Liao, S.; Chen, F.; Yang, Q.; Wang, D.-Y. Role of IL-25, IL-33, and TSLP in triggering united airway diseases toward type 2 inflammation. *Allergy* **2020**, *75*, 2794–2804. [CrossRef] [PubMed]
26. Kalchiem-Dekel, O.; Yao, X.; Barochia, A.V.; Kaler, M.; Figueroa, D.M.; Karkowsky, W.B.; Gordon, E.M.; Gao, M.; Fergusson, M.M.; Qu, X.; et al. Apolipoprotein E Signals via TLR4 to Induce CXCL5 Secretion by Asthmatic Airway Epithelial Cells. *Am. J. Respir. Cell Mol. Biol.* **2020**, *63*, 185–197. [CrossRef] [PubMed]

27. Hong, G.H.; Kwon, H.-S.; Lee, K.Y.; Ha, E.H.; Moon, K.-A.; Kim, S.W.; Oh, W.; Kim, T.-B.; Moon, H.-B.; Cho, Y.S. hMSCs suppress neutrophil-dominant airway inflammation in a murine model of asthma. *Exp. Mol. Med.* **2017**, *49*, e288. [CrossRef]
28. Busse, P.J.; Birmingham, J.M.; Calatroni, A.; Manzi, J.; Goryachokovsky, A.; Fontela, G.; Federman, A.D.; Wisnivesky, J.P. Effect of aging on sputum inflammation and asthma control. *J. Allergy Clin. Immunol.* **2017**, *139*, 1808–1818.e1806. [CrossRef]
29. Sokulsky, L.A.; Garcia-Netto, K.; Nguyen, T.H.; Girkin, J.L.N.; Collison, A.; Mattes, J.; Kaiko, G.; Liu, C.; Bartlett, N.W.; Yang, M.; et al. A Critical Role for the CXCL3/CXCL5/CXCR2 Neutrophilic Chemotactic Axis in the Regulation of Type 2 Responses in a Model of Rhinoviral-Induced Asthma Exacerbation. *J. Immunol.* **2020**, *205*, 2468–2478. [CrossRef]
30. Choi, Y.; Kim, Y.M.; Lee, H.R.; Mun, J.; Sim, S.; Lee, D.; Le Pham, D.; Kim, S.; Shin, Y.S.; Lee, S.; et al. Eosinophil extracellular traps activate type 2 innate lymphoid cells through stimulating airway epithelium in severe asthma. *Allergy* **2020**, *75*, 95–103. [CrossRef]
31. Vedel-Krogh, S.; Rasmussen, K.L.; Nordestgaard, B.G.; Nielsen, S.F. Complement C3 and allergic asthma: A cohort study of the general population. *Eur. Respir. J.* **2021**, *57*, 2000645. [CrossRef] [PubMed]
32. Wang, R.; Cleary, R.A.; Wang, T.; Li, J.; Tang, D.D. The Association of Cortactin with Profilin-1 Is Critical for Smooth Muscle Contraction. *J. Biol. Chem.* **2014**, *289*, 14157–14169. [CrossRef] [PubMed]
33. Whitsett, J.A. Airway Epithelial Differentiation and Mucociliary Clearance. *Ann. Am. Thorac. Soc.* **2018**, *15* (Suppl. S3), S143–S148. [CrossRef] [PubMed]
34. Tanabe, T.; Rubin, B.K. Airway Goblet Cells Secrete Pro-Inflammatory Cytokines, Chemokines, and Growth Factors. *Chest* **2016**, *149*, 714–720. [CrossRef] [PubMed]
35. Hellings, P.W.; Steelant, B. Epithelial barriers in allergy and asthma. *J. Allergy Clin. Immunol.* **2020**, *145*, 1499–1509. [CrossRef]
36. Zhu, T.; Chen, Z.; Chen, G.; Wang, D.; Tang, S.; Deng, H.; Wang, J.; Li, S.; Lan, J.; Tong, J.; et al. Curcumin Attenuates Asthmatic Airway Inflammation and Mucus Hypersecretion Involving a PPARgamma-Dependent NF-kappaB Signaling Pathway In Vivo and In Vitro. *Mediat. Inflamm.* **2019**, *2019*, 4927430. [CrossRef]
37. Patil, R.H.; Naveen Kumar, M.; Kiran Kumar, K.M.; Nagesh, R.; Kavya, K.; Babu, R.; Ramesh, G.T.; Sharma, S.C. Dexamethasone inhibits inflammatory response via down regulation of AP-1 transcription factor in human lung epithelial cells. *Gene* **2018**, *645*, 85–94. [CrossRef]
38. Guo, M.; Liu, Y.; Han, X.; Han, F.; Zhu, J.; Zhu, S.; Chen, B. Tobacco smoking aggravates airway inflammation by upregulating endothelin-2 and activating the c-Jun amino terminal kinase pathway in asthma. *Int. Immunopharmacol.* **2019**, *77*, 105916. [CrossRef]
39. Zeng, Z.; Wang, L.; Ma, W.; Zheng, R.; Zhang, H.; Zeng, X.; Zhang, H.; Zhang, W. Inhibiting the Notch signaling pathway suppresses Th17-associated airway hyperresponsiveness in obese asthmatic mice. *Lab. Investig.* **2019**, *99*, 1784–1794. [CrossRef]
40. Feng, J.; Zhang, C.; Wang, Z.; Li, Q.; Li, J.; Wang, H. Association betweenCD14gene promoter polymorphisms with serum total-IgE and eosinophil levels in atopic and non-atopic asthma patients in a Chinese Han population. *J. Asthma* **2016**, *53*, 119–124. [CrossRef]
41. Hachim, M.Y.; Elemam, N.M.; Ramakrishnan, R.K.; Salameh, L.; Olivenstein, R.; Hachim, I.Y.; Venkatachalam, T.; Mahboub, B.; Al Heialy, S.; Halwani, R.; et al. Blood and Salivary Amphiregulin Levels as Biomarkers for Asthma. *Front. Med.* **2020**, *7*, 561866. [CrossRef] [PubMed]
42. Schaefer, N.; Li, X.; Seibold, M.A.; Jarjour, N.N.; Denlinger, L.C.; Castro, M.; Coverstone, A.M.; Teague, W.G.; Boomer, J.; Bleecker, E.R.; et al. The effect of BPIFA1/SPLUNC1 genetic variation on its expression and function in asthmatic airway epithelium. *JCI Insight.* **2019**, *4*, e127237. [CrossRef] [PubMed]
43. Wong, S.L.; To, J.; Santos, J.; Allam, V.S.R.R.; Dalton, J.P.; Jordjevic, S.P.; Donnelly, S.; Padula, M.P.; Sukkar, M.B. Proteomic Analysis of Extracellular HMGB1 Identifies Binding Partners and Exposes Its Potential Role in Airway Epithelial Cell Homeostasis. *J. Proteome Res.* **2018**, *17*, 33–45. [CrossRef] [PubMed]
44. Singhania, A.; Wallington, J.C.; Smith, C.G.; Horowitz, D.; Staples, K.J.; Howarth, P.H.; Gadola, S.D.; Djukanović, R.; Woelk, C.; Hinks, T.S.C. Multitissue Transcriptomics Delineates the Diversity of Airway T Cell Functions in Asthma. *Am. J. Respir. Cell Mol. Biol.* **2018**, *58*, 261–270. [CrossRef]
45. Lkhagvadorj, K.; Meyer, K.F.; Verweij, L.P.; Kooistra, W.; Reinders-Luinge, M.; Dijkhuizen, H.W.; de Graaf, I.A.M.; Plösch, T.; Hylkema, M.N. Prenatal smoke exposure induces persistent Cyp2a5 methylation and increases nicotine metabolism in the liver of neonatal and adult male offspring. *Epigenetics* **2020**, *15*, 1370–1385. [CrossRef]
46. A Sokulsky, L.; Goggins, B.; Sherwin, S.; Eyers, F.; E Kaiko, G.; Board, P.G.; Keely, S.; Yang, M.; Foster, P.S. GSTO1-1 is an upstream suppressor of M2 macrophage skewing and HIF-1α-induced eosinophilic airway inflammation. *Clin. Exp. Allergy.* **2020**, *50*, 609–624. [CrossRef]
47. Lin, T.-J.; Karmaus, W.J.; Chen, M.-L.; Hsu, J.-C.; Wang, I.-J. Interactions Between Bisphenol A Exposure andGSTP1Polymorphisms in Childhood Asthma. *Allergy Asthma Immunol. Res.* **2018**, *10*, 172–179. [CrossRef]
48. Choi, H.; Song, W.-M.; Wang, M.; Sram, R.J.; Zhang, B. Benzo[a]pyrene is associated with dysregulated myelo-lymphoid hematopoiesis in asthmatic children. *Environ. Int.* **2019**, *128*, 218–232. [CrossRef]
49. Poulain-Godefroy, O.; Boute, M.; Carrard, J.; Alvarez-Simon, D.; Tsicopoulos, A.; de Nadai, P. The Aryl Hydrocarbon Receptor in Asthma: Friend or Foe? *Int. J. Mol. Sci.* **2020**, *21*, 8797. [CrossRef]
50. Shang, L.; Wang, L.; Shi, X.; Wang, N.; Zhao, L.; Wang, J.; Liu, C. HMGB1 was negatively regulated by HSF1 and mediated the TLR4/MyD88/NF-kappaB signal pathway in asthma. *Life Sci.* **2020**, *241*, 117120. [CrossRef]

51. Simpson, J.; Loh, Z.; Ullah, M.A.; Lynch, J.P.; Werder, R.B.; Collinson, N.; Zhang, V.; Dondelinger, Y.; Bertrand, M.; Everard, M.; et al. Respiratory Syncytial Virus Infection Promotes Necroptosis and HMGB1 Release by Airway Epithelial Cells. *Am. J. Respir. Crit. Care Med.* **2020**, *201*, 1358–1371. [CrossRef] [PubMed]
52. Todd, J.L.; Kelly, F.L.; Nagler, A.; Banner, K.; Pavlisko, E.N.; Belperio, J.A.; Brass, D.; Weigt, S.S.; Palmer, S. Amphiregulin contributes to airway remodeling in chronic allograft dysfunction after lung transplantation. *Am. J. Transplant.* **2020**, *20*, 825–833. [CrossRef] [PubMed]
53. Nordgren, T.; Heires, A.J.; Bailey, K.L.; Katafiasz, D.M.; Toews, M.L.; Wichman, C.S.; Romberger, D.J. Docosahexaenoic acid enhances amphiregulin-mediated bronchial epithelial cell repair processes following organic dust exposure. *Am. J. Physiol. Cell. Mol. Physiol.* **2018**, *314*, L421–L431. [CrossRef] [PubMed]
54. Cui, H.; Banerjee, S.; Guo, S.; Xie, N.; Ge, J.; Jiang, D.; Zörnig, M.; Thannickal, V.J.; Liu, G. Long noncoding RNA Malat1 regulates differential activation of macrophages and response to lung injury. *JCI Insight* **2019**, *4*, e124522. [CrossRef]
55. Lin, L.; Li, Q.; Hao, W.; Zhang, Y.; Zhao, L.; Han, W. Upregulation of LncRNA Malat1 Induced Proliferation and Migration of Airway Smooth Muscle Cells via miR-150-eIF4E/Akt Signaling. *Front. Physiol.* **2019**, *10*, 1337. [CrossRef]
56. Rohde, D.; Schön, C.; Boerries, M.; Didrihsone, I.; Ritterhoff, J.; Kubatzky, K.F.; Völkers, M.; Herzog, N.; Mähler, M.; Tsoporis, J.N.; et al. S100A1 is released from ischemic cardiomyocytes and signals myocardial damage via Toll-like receptor 4. *EMBO Mol. Med.* **2014**, *6*, 778–794. [CrossRef]
57. Brinks, H.; Rohde, D.; Voelkers, M.; Qiu, G.; Pleger, S.T.; Herzog, N.; Rabinowitz, J.; Ruhparwar, A.; Silvestry, S.; Lerchenmüller, C.; et al. S100A1 Genetically Targeted Therapy Reverses Dysfunction of Human Failing Cardiomyocytes. *J. Am. Coll. Cardiol.* **2011**, *58*, 966–973. [CrossRef]
58. Ma, W.-Y.; Song, R.-J.; Xu, B.-B.; Xu, Y.; Wang, X.-X.; Sun, H.-Y.; Li, S.-N.; Liu, S.-Z.; Yu, M.-X.; Yang, F.; et al. Melatonin promotes cardiomyocyte proliferation and heart repair in mice with myocardial infarction via miR-143-3p/Yap/Ctnnd1 signaling pathway. *Acta Pharmacol. Sin.* **2021**, *42*, 921–931. [CrossRef]
59. Kim, H.G.; Huang, M.; Xin, Y.; Zhang, Y.; Zhang, X.; Wang, G.; Liu, S.; Wan, J.; Ahmadi, A.R.; Sun, Z.; et al. The epigenetic regulator SIRT6 protects the liver from alcohol-induced tissue injury by reducing oxidative stress in mice. *J. Hepatol.* **2019**, *71*, 960–969. [CrossRef]
60. Rawlins, E.L.; Okubo, T.; Xue, Y.; Brass, D.M.; Auten, R.L.; Hasegawa, H.; Wang, F.; Hogan, B.L. The Role of Scgb1a1+ Clara Cells in the Long-Term Maintenance and Repair of Lung Airway, but Not Alveolar, Epithelium. *Cell Stem Cell* **2009**, *4*, 525–534. [CrossRef]
61. Brasier, A.R. Therapeutic targets for inflammation-mediated airway remodeling in chronic lung disease. *Expert Rev. Respir. Med.* **2018**, *12*, 931–939. [CrossRef] [PubMed]
62. Habiel, D.M.; Camelo, A.; Espindola, M.; Burwell, T.; Hanna, R.; Miranda, E.; Carruthers, A.; Bell, M.; Coelho, A.L.; Liu, H.; et al. Divergent roles for Clusterin in Lung Injury and Repair. *Sci. Rep.* **2017**, *7*, 15444. [CrossRef] [PubMed]
63. Hong, J.; Kim, M.N.; Kim, E.G.; Lee, J.; Kim, H.; Kim, S.; Lee, S.; Kim, Y.; Kim, K.; Sohn, M. Clusterin Deficiency Exacerbates Hyperoxia-Induced Acute Lung Injury. *Cells* **2021**, *10*, 944. [CrossRef] [PubMed]
64. Lauzon-Joset, J.-F.; Langlois, A.; Lai, L.J.; Santerre, K.; Lee-Gosselin, A.; Bossé, Y.; Marsolais, D.; Bissonnette, E.Y. Lung CD200 Receptor Activation Abrogates Airway Hyperresponsiveness in Experimental Asthma. *Am. J. Respir. Cell Mol. Biol.* **2015**, *53*, 276–284. [CrossRef] [PubMed]
65. Baos, S.; Calzada, D.; Cremades-Jimeno, L.; de Pedro, M.; Sastre, J.; Picado, C.; Quiralte, J.; Florido, F.; Lahoz, C.; Cárdaba, B. Discriminatory Molecular Biomarkers of Allergic and Nonallergic Asthma and Its Severity. *Front. Immunol.* **2019**, *10*, 1051. [CrossRef] [PubMed]
66. Cardenas, A.; Sordillo, J.E.; Rifas-Shiman, S.L.; Chung, W.; Liang, L.; Coull, B.A.; Hivert, M.-F.; Lai, P.S.; Forno, E.; Celedón, J.C.; et al. The nasal methylome as a biomarker of asthma and airway inflammation in children. *Nat. Commun.* **2019**, *10*, 3095. [CrossRef]
67. Xu, Y.; Wang, Y.; Besnard, V.; Ikegami, M.; Wert, S.E.; Heffner, C.; Murray, S.A.; Donahue, L.R.; Whitsett, J.A. Transcriptional Programs Controlling Perinatal Lung Maturation. *PLoS ONE* **2012**, *7*, e37046. [CrossRef]
68. Little, D.R.; Lynch, A.M.; Yan, Y.; Akiyama, H.; Kimura, S.; Chen, J. Differential chromatin binding of the lung lineage transcription factor NKX2-1 resolves opposing murine alveolar cell fates in vivo. *Nat. Commun.* **2021**, *12*, 1–18. [CrossRef]
69. Zhou, P.; Gu, F.; Zhang, L.; Akerberg, B.N.; Ma, Q.; Li, K.; He, A.; Lin, Z.; Stevens, S.M.; Zhou, B.; et al. Mapping cell type-specific transcriptional enhancers using high affinity, lineage-specific Ep300 bioChIP-seq. *eLife* **2017**, *6*, 166. [CrossRef]
70. Hohl, M.; Thiel, G. Cell type-specific regulation of RE-1 silencing transcription factor (REST) target genes. *Eur. J. Neurosci.* **2005**, *22*, 2216–2230. [CrossRef]
71. Lemeille, S.; Paschaki, M.; Baas, D.; Morlé, L.; Duteyrat, J.-L.; Ait-Lounis, A.; Barras, E.; Soulavie, F.; Jerber, J.; Thomas, J.; et al. Interplay of RFX transcription factors 1, 2 and 3 in motile ciliogenesis. *Nucleic Acids Res.* **2020**, *48*, 9019–9036. [CrossRef] [PubMed]
72. Patir, A.; Fraser, A.M.; Barnett, M.W.; McTeir, L.; Rainger, J.; Davey, M.G.; Freeman, T.C. The transcriptional signature associated with human motile cilia. *Sci. Rep.* **2020**, *10*, 1081. [CrossRef] [PubMed]
73. Besnard, V.; Wert, S.E.; Kaestner, K.H.; Whitsett, J.A. Stage-specific regulation of respiratory epithelial cell differentiation by Foxa1. *Am. J. Physiol. Cell. Mol. Physiol.* **2005**, *289*, L750–L759. [CrossRef] [PubMed]
74. Mümmler, C.; Burgy, O.; Hermann, S.; Mutze, K.; Günther, A.; Königshoff, M. Cell-specific expression of runt-related transcription factor 2 contributes to pulmonary fibrosis. *FASEB J.* **2018**, *32*, 703–716. [CrossRef] [PubMed]

75. Paranjapye, A.; Mutolo, M.J.; Ebron, J.S.; Leir, S.-H.; Harris, A. The FOXA1 transcriptional network coordinates key functions of primary human airway epithelial cells. *Am. J. Physiol. Cell. Mol. Physiol.* **2020**, *319*, L126–L136. [CrossRef] [PubMed]
76. Zhu, J.; Wang, K.; Li, T.; Chen, J.; Xie, D.; Chang, X.; Yao, J.; Wu, J.; Zhou, Q.; Jia, Y.; et al. Hypoxia-induced TET1 facilitates trophoblast cell migration and invasion through HIF1α signaling pathway. *Sci. Rep.* **2017**, *7*, 807. [CrossRef]
77. Ali, M.M.; Phillips, S.A.; Mahmoud, A.M. HIF1alpha/TET1 Pathway Mediates Hypoxia-Induced Adipocytokine Promoter Hypomethylation in Human Adipocytes. *Cells* **2020**, *9*, 134. [CrossRef]
78. Johnsen, O.; Skammelsrud, N.; Luna, L.; Nishizawa, M.; Prydz, H.; Kolsto, A.B. Small Maf proteins interact with the human transcription factor TCF11/Nrf1/LCR-F1. *Nucleic Acids Res.* **1996**, *24*, 4289–4297. [CrossRef]
79. Steffen, J.; Seeger, M.; Koch, A.; Krüger, E. Proteasomal Degradation Is Transcriptionally Controlled by TCF11 via an ERAD-Dependent Feedback Loop. *Mol. Cell* **2010**, *40*, 147–158. [CrossRef]
80. Radhakrishnan, S.K.; den Besten, W.; Deshaies, R.J. p97-Dependent retrotranslocation and proteolytic processing govern formation of active Nrf1 upon proteasome inhibition. *Elife* **2014**, *3*, e01856. [CrossRef]
81. Tonelli, C.; Chio, I.I.C.; Tuveson, D.A. Transcriptional Regulation by Nrf2. *Antioxid. Redox Signal.* **2018**, *29*, 1727–1745. [CrossRef] [PubMed]
82. Kawakita, N.; Toba, H.; Miyoshi, K.; Sakamoto, S.; Matsumoto, D.; Takashima, M.; Aoyama, M.; Inoue, S.; Morimoto, M.; Nishino, T.; et al. Bronchioalveolar stem cells derived from mouse-induced pluripotent stem cells promote airway epithelium regeneration. *Stem Cell Res. Ther.* **2020**, *11*, 430. [CrossRef] [PubMed]
83. Hogan, B.L.; Barkauskas, C.E.; Chapman, H.A.; Epstein, J.A.; Jain, R.; Hsia, C.C.; Niklason, L.; Calle, E.; Le, A.; Randell, S.H.; et al. Repair and Regeneration of the Respiratory System: Complexity, Plasticity, and Mechanisms of Lung Stem Cell Function. *Cell Stem Cell* **2014**, *15*, 123–138. [CrossRef] [PubMed]
84. Gon, Y.; Hashimoto, S. Role of airway epithelial barrier dysfunction in pathogenesis of asthma. *Allergol. Int.* **2018**, *67*, 12–17. [CrossRef] [PubMed]
85. Huang, J.; Yue, H.; Jiang, T.; Gao, J.; Shi, Y.; Shi, B.; Wu, X.; Gou, X. IL-31 plays dual roles in lung inflammation in an OVA-induced murine asthma model. *Biol. Open* **2019**, *8*, bio036244. [CrossRef]
86. Flayer, C.H.; Ge, M.Q.; Hwang, J.W.; Kokalari, B.; Redai, I.G.; Jiang, Z.; Haczku, A. Ozone Inhalation Attenuated the Effects of Budesonide on Aspergillus fumigatus-Induced Airway Inflammation and Hyperreactivity in Mice. *Front. Immunol.* **2019**, *10*, 2173. [CrossRef] [PubMed]
87. Golebski, K.; Luiten, S.; Van Egmond, D.; De Groot, E.; Röschmann, K.I.L.; Fokkens, W.J.; Van Drunen, C.M. High Degree of Overlap between Responses to a Virus and to the House Dust Mite Allergen in Airway Epithelial Cells. *PLoS ONE* **2014**, *9*, e87768. [CrossRef]
88. Liu, B.; Sun, H.; Wang, J.; Liu, H.; Zhao, C. Potential role for EZH2 in promotion of asthma through suppression of miR-34b transcription by inhibition of FOXO3. *Lab. Investig.* **2021**, *101*, 998–1010. [CrossRef]
89. Ravanetti, L.; Dijkhuis, A.; Dekker, T.; Pineros, Y.S.S.; Ravi, A.; Dierdorp, B.S.; Erjefält, J.S.; Mori, M.; Pavlidis, S.; Adcock, I.M.; et al. IL-33 drives influenza-induced asthma exacerbations by halting innate and adaptive antiviral immunity. *J. Allergy Clin. Immunol.* **2019**, *143*, 1355–1370.e1316. [CrossRef]
90. Li, R.; Wang, J.; Zhu, F.; Li, R.; Liu, B.; Xu, W.; He, G.; Cao, H.; Wang, Y.; Yang, J. HMGB1 regulates T helper 2 and T helper17 cell differentiation both directly and indirectly in asthmatic mice. *Mol. Immunol.* **2018**, *97*, 45–55. [CrossRef]
91. Fribley, A.; Zhang, K.; Kaufman, R.J. Regulation of Apoptosis by the Unfolded Protein Response. In *Methods in Molecular Biology*; Humana Press: Totowa, NJ, USA, 2009; Volume 559, pp. 191–204.
92. Pathinayake, P.S.; Hsu, A.C.-Y.; Waters, D.W.; Hansbro, P.; Wood, L.G.; Wark, P. Understanding the Unfolded Protein Response in the Pathogenesis of Asthma. *Front. Immunol.* **2018**, *9*, 175. [CrossRef] [PubMed]
93. Yaghi, A.; Dolovich, M.B. Airway Epithelial Cell Cilia and Obstructive Lung Disease. *Cells* **2016**, *5*, 40. [CrossRef] [PubMed]
94. Thomas, B.; Rutman, A.; Hirst, R.A.; Haldar, P.; Wardlaw, A.; Bankart, J.; Brightling, C.; O'Callaghan, C. Ciliary dysfunction and ultrastructural abnormalities are features of severe asthma. *J. Allergy Clin. Immunol.* **2010**, *126*, 722.e2–729.e2. [CrossRef] [PubMed]
95. Aizawa, H.; Koarai, A.; Shishikura, Y.; Yanagisawa, S.; Yamaya, M.; Sugiura, H.; Numakura, T.; Yamada, M.; Ichikawa, T.; Fujino, N.; et al. Oxidative stress enhances the expression of IL-33 in human airway epithelial cells. *Respir Res.* **2018**, *19*, 52. [CrossRef]
96. Wan, H.; Dingle, S.; Xu, Y.; Besnard, V.; Kaestner, K.H.; Ang, S.-L.; Wert, S.; Stahlman, M.T.; Whitsett, J.A. Compensatory Roles of Foxa1 and Foxa2 during Lung Morphogenesis. *J. Biol. Chem.* **2005**, *280*, 13809–13816. [CrossRef]
97. Sun, Z.; Xu, X.; He, J.; Murray, A.; Sun, M.; Wei, X.; Wang, X.; McCoig, E.; Xie, E.; Jiang, X.; et al. EGR1 recruits TET1 to shape the brain methylome during development and upon neuronal activity. *Nat. Commun.* **2019**, *10*, 3892. [CrossRef]
98. Yang, Y.A.; Zhao, J.C.; Fong, K.-W.; Kim, J.; Li, S.; Song, C.-X.; Song, B.; Zheng, B.; He, C.; Yu, J. FOXA1 potentiates lineage-specific enhancer activation through modulating TET1 expression and function. *Nucleic Acids Res.* **2016**, *44*, 8153–8164. [CrossRef]

A

Treatment Protocol			
HDM	(I.P)	1d and 7d	100μg HDM+100μg Alum +100μl Saline
	(I.T)	17d, 19d, and 21d	100μg HDM+50μl Saline
Saline	(I.P)	1d and 7d	100μl Saline
	(I.T)	17d, 19d, and 21d	50μl Saline

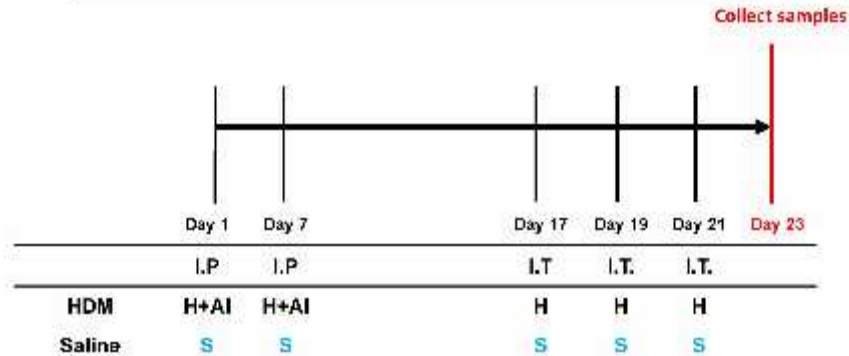

B

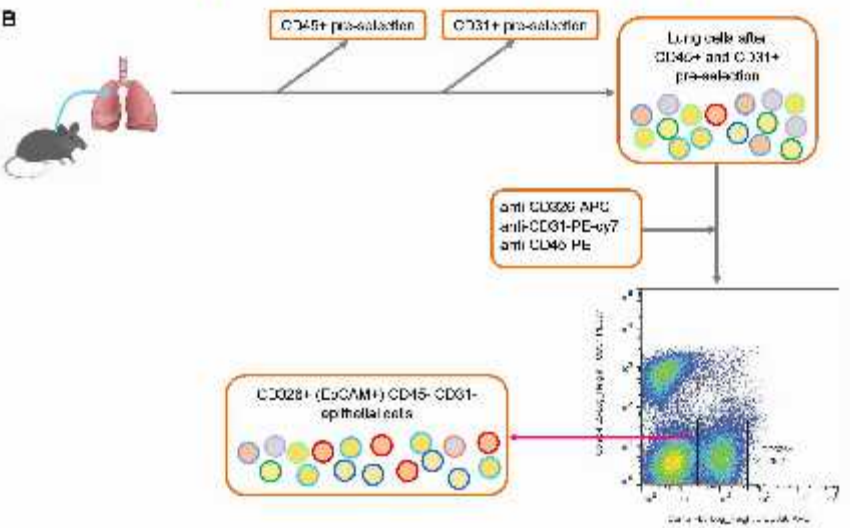

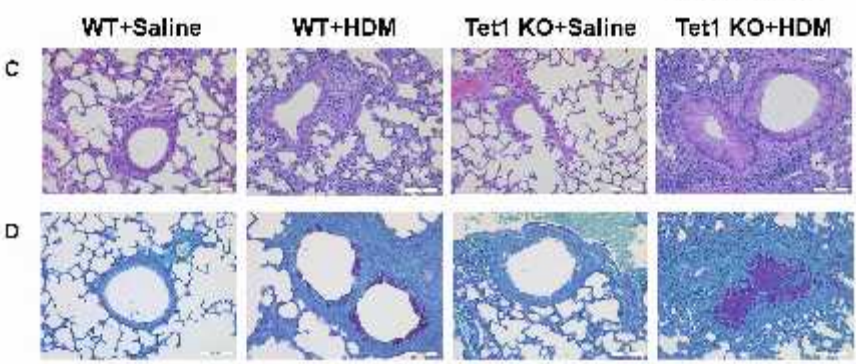

Supplementary Figure 1

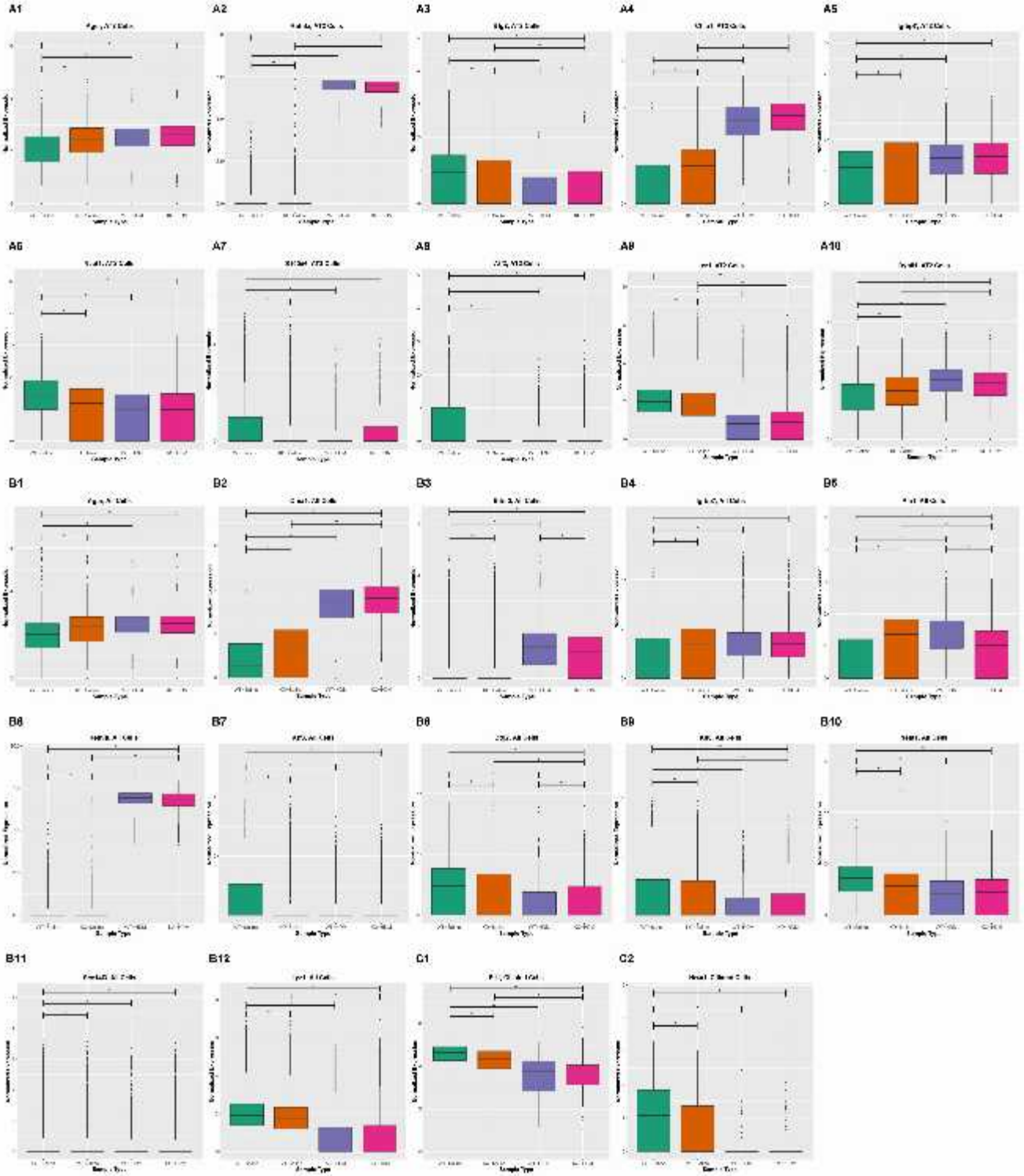

Supplementary Figure 3

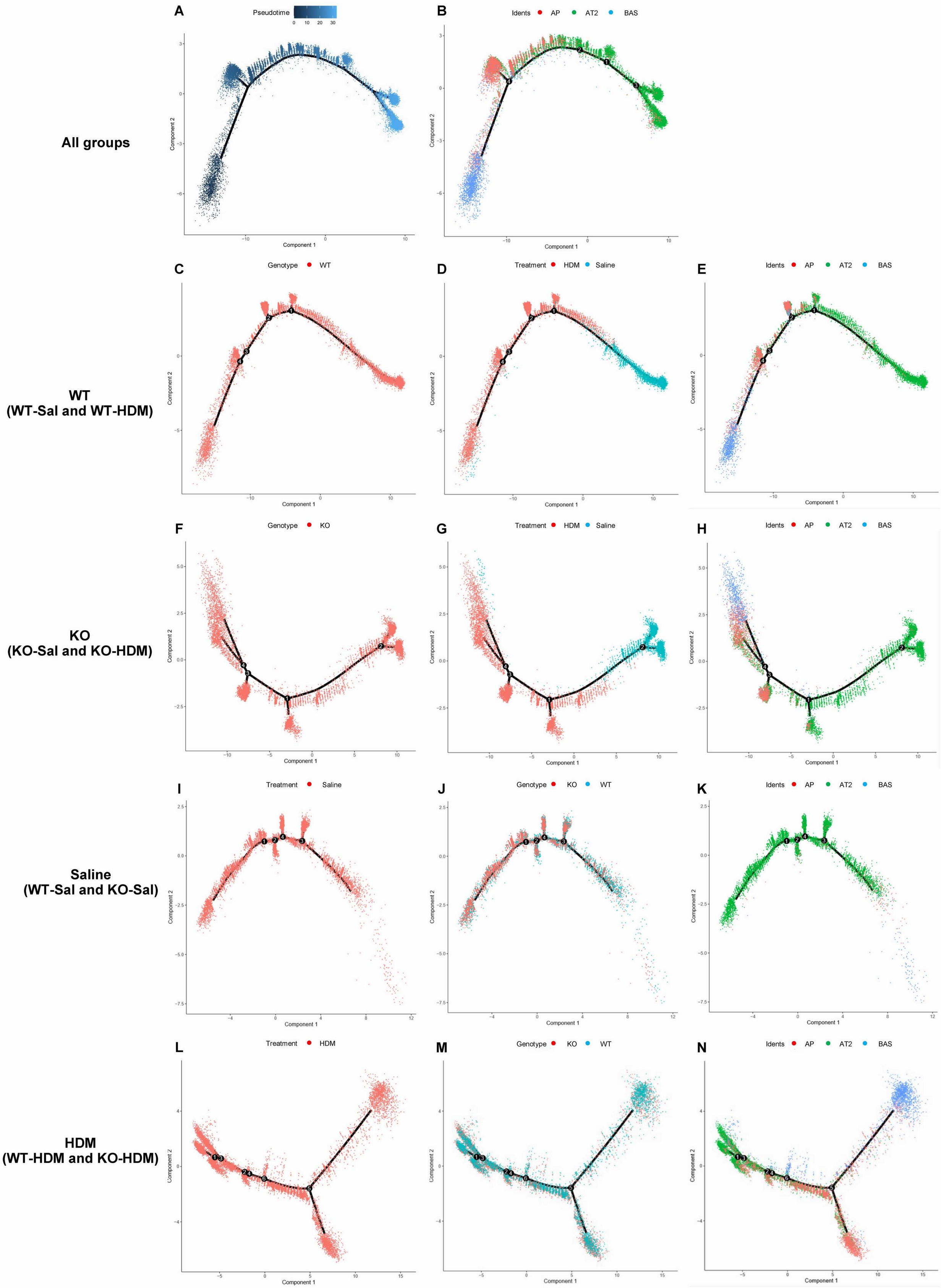

Supplementary Figure 4

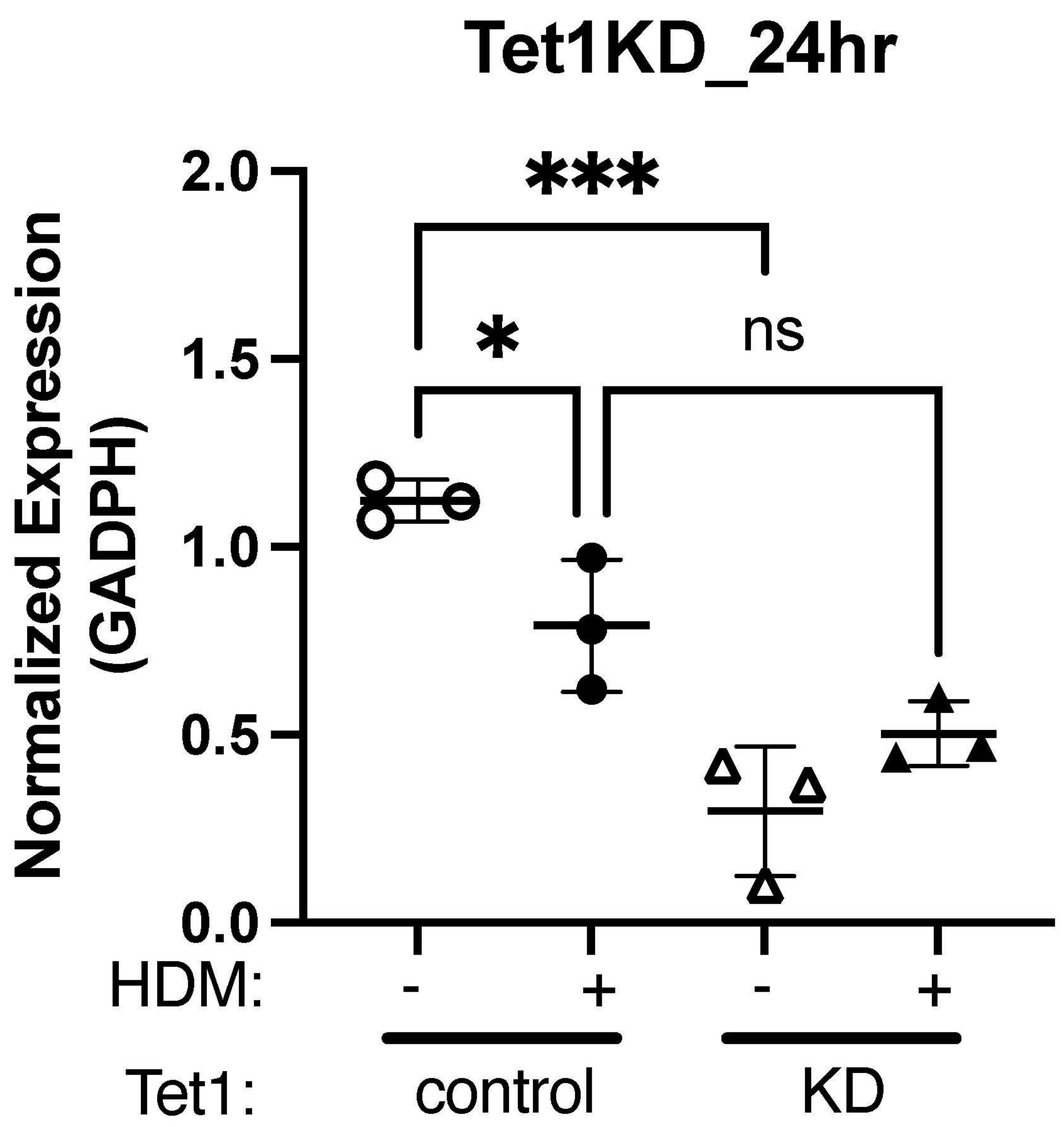

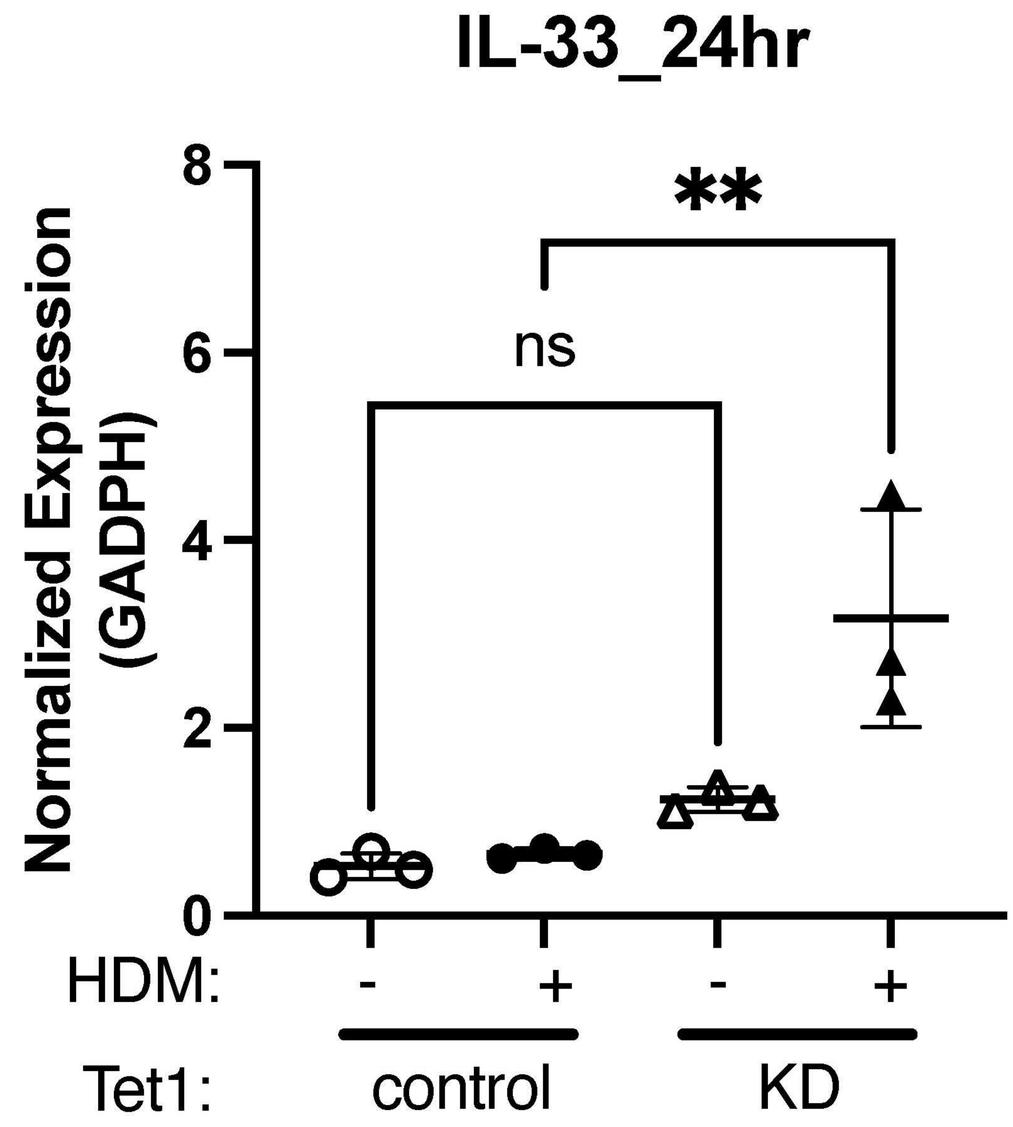

Supplementary Figure 6

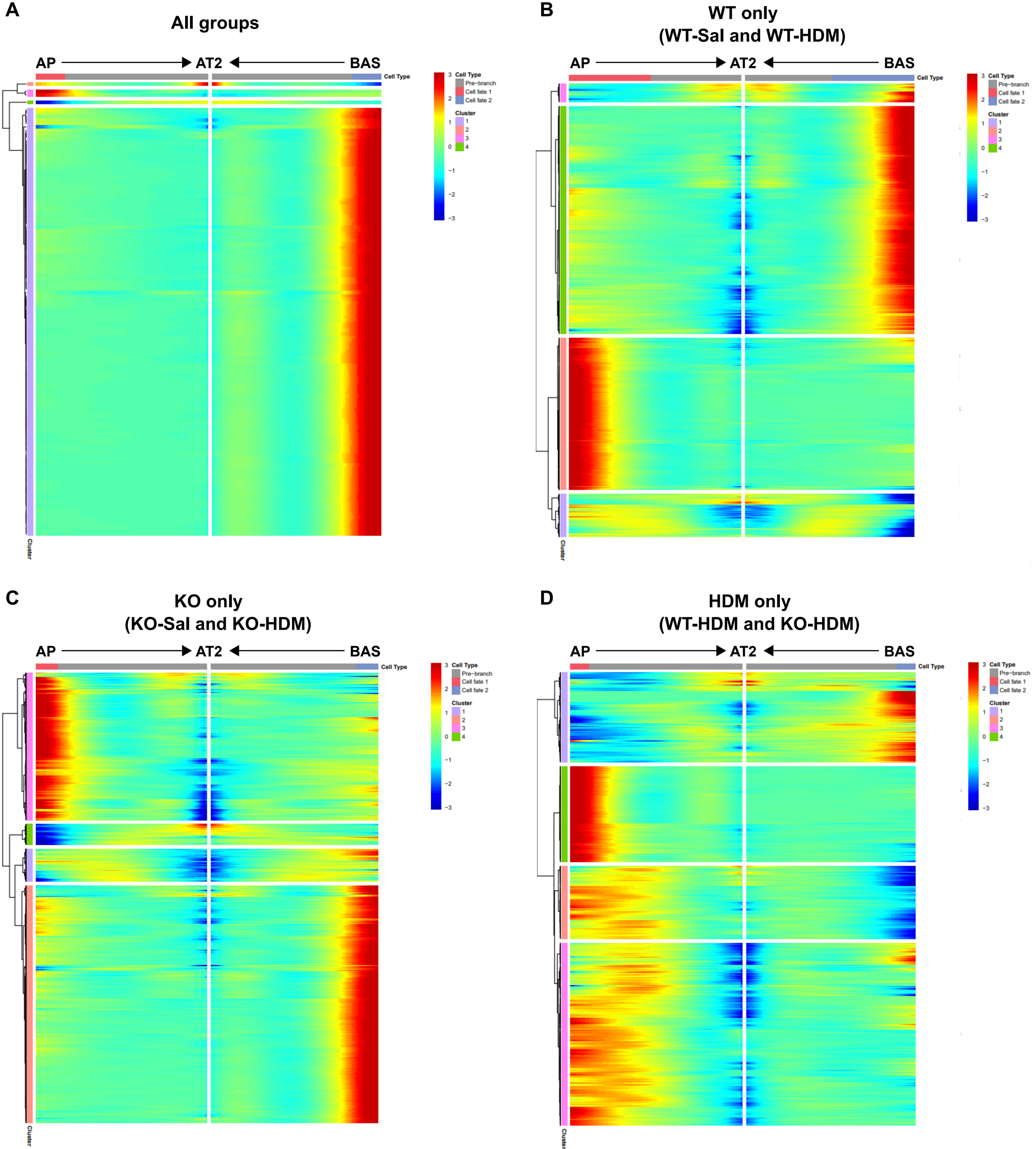
A
All groups
AP
AT2
BAS
Cell Type
Cluster
Pre−branch
Cell fate 1
Cell fate 2
B
WT only
(WT-Sal and WT-HDM)
C
KO only
(KO-Sal and KO-HDM)
D
HDM only
(WT-HDM and KO-HDM)

Supplementary Methods

Animal

In this study, both Tet1$^{-/-}$ mice (knockout/KO mice) and their littermate Tet1$^{+/+}$ mice (wildtype/WT mice) were used. The establishment of Tet1$^{-/-}$ mouse was described in a previous study [9]. Meanwhile, all procedures on animals were approved by the Animal Experimental Ethics Committee of Cincinnati Children's Hospital Medical Center and University of California, Davis. This study was performed based on the recommendations in the Guide for the Care and Use of Laboratory Animals. All surgery was performed under anesthesia, and all efforts were made to minimize suffering. Specific pathogen free (SPF) mice (16-24g, age 8-12 weeks, n=2 for all four groups), were maintained under SPF conditions in the animal facilities. The mice were fed in a temperature-controlled room (12-h dark and light cycles) and offered *ad libitum* access to food and water. Animals underwent an acclimatization period of at least 1 week before the study.

Murine model of HDM-induced allergic airway inflammation

In this study, the murine asthma model was induced by HDM as we previously described [9] (Figure S1A). Mice in the WT-HDM and KO-HDM groups were challenged with two intraperitoneal (I.P) injections of 100μg HDM [including 61.3μg of protein, Dermatophagoides pteronyssinus, Greer Laboratories (Lenoir, NC)] plus 100μg aluminium (Alum) in 100μl Saline followed by three intratracheal (I.T) instillations of 100μg HDM in 50μl Saline. Meanwhile, mice in the WT-Saline and KO-Saline groups were treated with 50μl Saline instead of HDM. To ensure the successful establishment of the mouse model, the left caudal lung of each mouse was fixed in 10% formalin, embedded in paraffin, and cut into 5μm sections. Hematoxylin and eosin (H&E) staining was performed to observe pulmonary pathological alterations. Periodic acid–Schiff (PAS) staining was used to observe goblet cell hyperplasia and airway mucus secretion.

Ingenuity pathway analysis In the current study, canonical pathway analysis and diseases and functions were carried out using the Ingenuity Pathway Analysis (IPA, Ingenuity Systems, Redwood City, CA). Meanwhile, statistical significance was set at $p<0.05$ (−log (P-value) >1.3).

HBECs growth and TET1 knockdown

HBEC were grown in 1X K-SFM supplemented with EGF, pituitary extract, and pen-strep (complete media). A 12 well plate was seeded with cultured HBEC with near confluent numbers and incubated overnight for attachment. After 24 hours, the complete media was replaced with 1X K-SFM with no serum supplements (minimal media) and incubated for an additional 8 hours. TET1 was knocked down by adding 30 pmol/mL siRNA (ThermoFisher) and incubated for 24 hours in minimal media. House dust mite (HDM, Greer) was added to HBEC at a concentration of 25ug/mL and incubated for another 24 hours. Cells were then collected for library preparation and RNA extraction for analysis. There were four different sample types in our study: 1) wildtype (WT) saline, 2) WT house dust mite (HDM), 3) TET1 knockdown (KD) saline, and 4) KD HDM.

RT-qPCR analysis

Total RNA was reverse-transcribed to cDNA using the VILO cDNA kit (Thermo Fisher Scientific, Waltham, MA, USA) according to the manufacturer's instructions. Real-time quantitative PCR was performed using the SYBR Green Master Kit and Quantstudio instrument. PCR was carried out in duplicates for each fraction and the mean Ct value of the triplicate reaction was normalized against the mean Ct value of GAPDH. TET1 forward: 5'-CCCGGGCTCCAAAGTTGTG-3'; Reverse, 5'-GCAGGAAACAGAGTCATTGGTCCT-3'. IL33 primers: Forward, 5'-CCT GTC AAC AGC AGT CTA C-3'; Reverse, 5'-TTG GCA TGC AAC CAG AAG TC-3'. GADPH primers: Forward, 5'-GGGGAAGGTGAAGGTCGGAGTCA-3'; Reverse, 5'-AGCCTTGACGGTGCCATGGAAT-3'.

Supplementary Figure Legends

Supplementary Figure S1.

(A) Treatment Protocol;

(B) Lung epithelial cells ($CD326^+$ $CD31^-$ $CD45^-$ cells) sorting. Representative sorting images (one from WT and one from KO are shown);

(C) and (D) Lung pathological alterations and airway mucus secretion in HDM-induced airway inflammation in mice. [(C) HE staining. The figure demonstrates a representative view (×200) from each group. (D) PAS staining. The figure demonstrates a representative view (×200) from each group.]

Supplementary Figure S2. Cell type-specific expression of *Epcam* and *Scgb1a1*. Boxplots showing the expression levels of (A) *Epcam*, (B) *Scgb1a1* and (c) *Tet1* for each epithelial cell type.

Supplementary Figure S3. The expressions of asthma-associated DEGs (WT-Sal vs WT-HDM, WT-Sal vs KO-Sal, and KO-HDM vs WT-Sal overlapped DEGs) in (A1-10) AT2 cells, (B1-12) $EpCAM^+$ lung epithelial cells, and (C1-2) ciliated cells.

Supplementary Figure S4. Single-cell trajectory analysis reveals the differentiation of AP and BAS cells into AT2 cells.

(A) and (B) Single-cell trajectory of AP, BAS, and AT2 cells in all mice.

(C), (D), and (E) Single-cell trajectory of AP, BAS, and AT2 cells in WT mice with saline treatment and HDM challenge.

(F), (G), and (H) Single-cell trajectory of AP, BAS, and AT2 cells in Tet1 KO mice with saline treatment and HDM challenge.

(I), (J), and (K) Single-cell trajectory of AP, BAS, and AT2 cells in WT and Tet1 KO mice with saline treatment.

(L), (M), and (N) Single-cell trajectory of AP, BAS, and AT2 cells in WT and Tet1 KO mice with HDM challenge.

Supplementary Figure S5. Expression heatmap of dynamically expressed genes ordered across single-cell trajectory analysis reveals the differentiation of AP cells and BAS into AT2 cells.

(A) Heatmap depicting genes with a branch-dependent manner for branch point 4 in all mice.

(B) Heatmap depicting genes with a branch-dependent manner for branch point 4 in WT mice with saline and HDM challenge.

(C) Heatmap depicting genes with a branch-dependent manner for branch point 3 in Tet1 KO mice with saline and HDM challenge.

(D) Heatmap depicting genes with a branch-dependent manner for branch point 5 in WT mice and Tet1 KO mice with HDM challenge.

Color scheme represents the z-score distribution from -3.0 (blue) to +3.0 (red). Each row represents the dynamic expression of a gene. Genes along the differentiation of AP cells and BAS into AT2 cells are clustered into 4 blocks. Cell types: Grey: AT2 cells, Red: AP cells, Blue: BAS.

Supplementary Figure S6. Impact of TET1 knockdown and HDM treatment in *IL33* expression in HBECs.

(A) TET1. (B) IL33.

* represents P<0.05; ** represents P<0.01; *** represents P<0.005; ns represents non significant.

Supplementary Tables

Supplementary Table S1. Markers used to define all the cell types.

Supplementary Table S2. Cell number in each group identified by scRNA-seq analysis.

Supplementary Table S3. Differentially expressed genes (DEGs) from bulk analysis (all EpCAM^{+} cells).

Supplementary Table S4. Enriched pathways with DEGs from bulk analysis by IPA analysis.

Supplementary Table S5. Differentially expressed genes from each cell type.

Supplementary Table S6. Examples of cell type-specific changes induced by HDM challenges and Tet1 loss.

"+" and "-" mean genes that were increased and decreased with a false discovery rate (FDR) ⩽0.05 and a fold change ⩾1.2.

N.S. (non-significant) means differential genes without a false discovery rate (FDR) ⩽0.05 and/or a fold change ⩾1.2.

N.E. (no-expression) means genes weren't detectable.

Supplementary Table S7. Enriched pathways with AT2-specific DEGs by IPA analysis.

Supplementary Table S8. Enriched pathways with ciliated cell-specific DEGs by IPA analysis.

Supplementary Table S9. Genes with the same directions of changes among WT-HDM vsWT-Sal, KO-SalvsWT-Sal, and KO-HDMvsWT-Sal.

Supplementary Table S10 Enriched pathways within genes with the same directions of changes among WT-HDM vs WT-Sal, KO-Sal vs WT-Sal, and KO-HDM vs WT-Sal in all EpCAM^{+} cells, AT2 cells, AP, BAS, and ciliated cells.

Supplementary Table S11. Enriched pathways within combined DEGs from all EpCAM^{+} cells, AT2 cells, AP, and BAS with the same directions of changes in KO-HDMvsWT-HDM.

Supplementary Table S2. Cell number in each group identified by scRNA-seq analysis

	WT-Sal	WT-HDM	KO-Sal	KO-HDM	Total
EpCAM^{+} cells	6378	6925	5420	6714	25437
AT1 cells	18 (0.282%)	5 (0.072%)	9 (0.166%)	8 (0.119%)	40 (0.157%)
AT2 cells	5502 (86.265%)	3885 (56.101%)	4572 (84.354%)	3770 (56.151%)	17729 (69.698%)
Alveolar progenitor cells	157 (2.462%)	1758 (25.386%)	84 (1.550%)	1905 (28.374%)	3904 (15.348%)
Broncho alveolar stem cells	55 (0.862%)	985 (14.224%)	62 (1.144%)	671 (9.994%)	1773 (6.970%)
Ciliated cells	362 (5.676%)	66 (0.953%)	189 (3.487%)	131 (1.951%)	748 (2.941%)
Stromal cells	105 (1.646%)	88 (1.271%)	354 (6.531%)	38 (0.566%)	585 (2.300%)
Club cells	95 (1.489%)	75 (1.083%)	115 (2.122%)	139 (2.070%)	424 (1.667%)
Goblet cells	5 (0.078%)	56 (0.809%)	20 (0.369%)	45 (0.670%)	126 (0.495%)
Neuroendocrine cells	79 (1.239%)	7 (0.101%)	15 (0.277%)	7 (0.104%)	108 (0.425%)

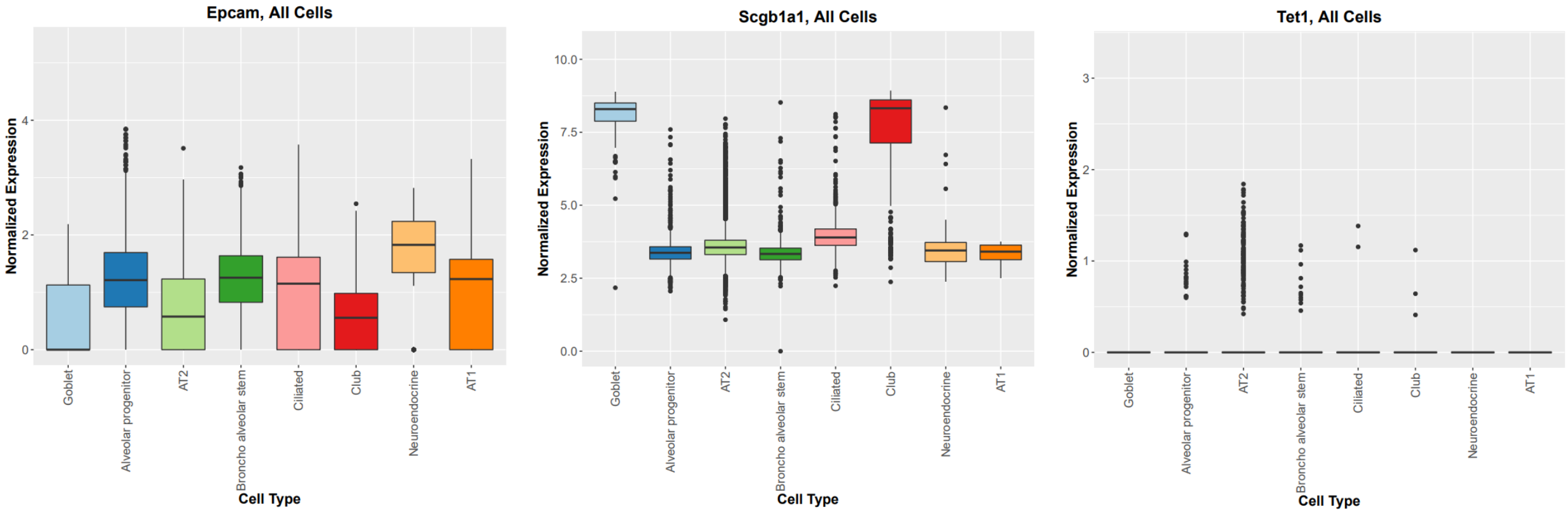

Supplementary Figure S2